CCM-80-1

Center for Composite Materials

PASSIVE THERMAL NONDESTRUCTIVE FLAW DETECTION IN COMPOSITES

DISTRIBUTION STATEMENT A
Approved for public release;
Distribution Unlimited

JOHN A. CHARLES
DALE W. WILSON

DEPARTMENT OF DEFENSE
PLASTICS TECHNICAL EVALUATION CENTER
ARRADCOM, DOVER, N. J. 07801

19951228 075

PLASTEC 34847

College of Engineering
University of Delaware
Newark, Delaware

111

-- 1 OF 3
-- ***DTIC DOES NOT HAVE THIS ITEM***
-- 1 - AD NUMBER: D433300
-- 5 - CORPORATE AUTHOR: DELAWARE UNIV NEWARK CENTER FOR COMPOSITE
-- MATERIALS
-- 6 - UNCLASSIFIED TITLE: INTERLAMINAR FLAW PROPAGATION MODE II,
--10 - PERSONAL AUTHORS: DIMONDI,V. ;
--11 - REPORT DATE: SEP , 1980
--12 - PAGINATION: 34P
--14 - REPORT NUMBER: CCM-80-18
--20 - REPORT CLASSIFICATION: UNCLASSIFIED
--22 - LIMITATIONS (ALPHA): APPROVED FOR PUBLIC RELEASE; DISTRIBUTION
-- UNLIMITED. AVAILABILITY:: CENTER FOR COMPOSITE MATERIALS,
-- UNIVERSITY OF DELAWARE, NEWARK, DE. 19711.
--33 - LIMITATION CODES: 1 24
--******
-- 2 OF 3
-- ***DTIC DOES NOT HAVE THIS ITEM***
-- 1 - AD NUMBER: D429478
-- 5 - CORPORATE AUTHOR: DELAWARE UNIV NEWARK CENTER FOR COMPOSITE
-- MATERIALS
-- 6 - UNCLASSIFIED TITLE: PASSIVE THERMAL NONDESTRUCTIVE FLAW
-- DETECTION IN COMPOSITES,

--10 - PERSONAL AUTHORS: CHARLES,J. A. ;WILSON,D. W. ;
--11 - REPORT DATE: AUG 18, 1979
--12 - PAGINATION: 84P
--14 - REPORT NUMBER: CCM-80-1
--20 - REPORT CLASSIFICATION: UNCLASSIFIED
--21 - SUPPLEMENTARY NOTE: PROJECT REPORT.
--22 - LIMITATIONS (ALPHA): APPROVED FOR PUBLIC RELEASE; DISTRIBUTION
-- UNLIMITED. AVAILABILITY: CENTER FOR COMPOSITE MATERIALS, UNIVERSITY
-- OF DELAWARE, 208 EVANS HALL, NEWARK, DE. 19711. REPT. 80-1.
--33 - LIMITATION CODES: 1 24
--******
-- 3 OF 3
-- ***DTIC DOES NOT HAVE THIS ITEM***
-- 1 - AD NUMBER: D310206
-- 5 - CORPORATE AUTHOR: DELAWARE UNIV NEWARK CENTER FOR COMPOSITE
-- MATERIALS
-- 6 - UNCLASSIFIED TITLE: PASSIVE THERMAL NONDESTRUCTIVE FLAW
-- DETECTION IN COMPOSITES
--10 - PERSONAL AUTHORS: CHARLES,JOHN A. ;WILSON,DALE W. ;
--11 - REPORT DATE: AUG , 1979
--12 - PAGINATION: 84P
--14 - REPORT NUMBER: CCM-80-1
--20 - REPORT CLASSIFICATION: UNCLASSIFIED

--22 - LIMITATIONS (ALPHA): AVAILABILITY. REQUEST FROM CENTER FOR
-- COMPOSITE MATERIALS, UNIVERSITY OF DELAWARE, NEWARK, DE 19711
--33 - LIMITATION CODES: 1
--******

"PASSIVE THERMAL NONDESTRUCTIVE FLAW DETECTION IN COMPOSITES"

PROJECT REPORT

John A. Charles

and

Dale W. Wilson

August 18, 1979

ABSTRACT

The use of passive thermal nondestructive testing for flaw detection in composite materials has been studied. Using implanted TFE and natural defects in fiberglass/epoxy and graphite/epoxy, techniques for generating and monitoring surface temperature distributions on composites were developed and refined. A radiant heat source was constructed to provide a uniform heat input to the back surface of the specimens while the temperature field on the front surface was visualized using liquid crystals. It was found that most internal defects can be found easily because of their effect on the surface temperature field.

In order to perform a parametric study of the problem, a numerical heat-transfer model was developed. Using this model, the important variables in the problem have been identified for continuing study. Furthermore, the model may also be used to predict the thermal behavior of any given system to aid in the proper selection of heat input and imaging system.

Through both the experimental and analytical work performed, it has been shown that thermal imaging with liquid crystals can be a viable method of flaw detection in composites. It is a fast, inexpensive and accurate tool for NDT in this important field.

DTIC QUALITY INSPECTED 3

TABLE OF CONTENTS

LIST OF FIGURES

(LIST OF FIGURES, continued)

INTRODUCTION

As composite materials continue to be developed, their unique properties and high strength-to-weight ratio make them increasingly more attractive to designers. The ability to tailor the strength properties of a component while reducing the overall weight of an assembly has led to widespread use of composites in the automotive and aircraft industries. However, barriers exist to the large-scale use of composites in primary load-carrying structures. One of these barriers is high cost; another is fabrication time and technology. A third barrier is the assurance of the integrity of the finished part. It is this third problem that is addressed in this report.

In attempting to ascertain the integrity of a part, it is essential that the tests performed be nondestructive. The art/science of nondestructive testing (NDT) has come to play an important role in composite material applications. Composites are susceptible to a number of unique kinds of damage, which can greatly decrease the strength of a part and render it useless. Among these kinds of damages are delaminations, debonding, fiber breakage, and matrix cracking . A complete NDT system should be capable of accurately locating and sizing damage in composites, whether the damage was the result of fabrication problems or in-service loading. Furthermore, it is desirable to have a

rapid NDT method for use in assembly-line situations. A simple system is attractive when it might be subjected to hard use or must be used by non-scientific personnel. Finally, the NDT methods used should be as inexpensive as possible to allow for their continuous, widespread use.

One system for NDT of composites under development which shows promise is thermal imaging, or "thermography." Thermography may be defined as the science (or art) of creating a visible image of temperatures on the surface of a body. There are several types of thermographic techniques, discerned by the means used in each to visualize surface temperatures. In general, however, thermographic methods may all be placed in one of two categories: (1) electronic imaging, and (2) chemical imaging.

In electronic thermal imaging, the photoelectric effect is used to convert infrared radiation (emitted from a body in proportion to the fourth power of its absolute temperature) into an electrical signal. The signal can then be interpreted to give surface temperatures. The most popular instrument for this type of imaging is the scanning infrared camera (SIRC). These instruments continuously scan the surface of an object and present the surface temperatures as shades of gray on a cathode-ray tube. SIRC's are capable of very high thermal and spatial resolution, and provide for easy data recording and interpretation through their electronic format. However, their complexity and high initial cost serves to inhibit the widespread utilization of SIRC's in industry.

The second category of thermal imaging is chemical. Into this category fall temperature sensitive papers and liquid crystals. Of these two, only liquid crystals provide a viable alternative to the more expensive SIRC described previously. Liquid crystals (LC) are available in several types, but only the group known as "cholesteric" possesses the unique property which allows it to be used for thermal imaging. These LC's behave mechanically as liquids and optically as solids. When subjected to different temperatures, cholesteric LC's change their structure in such a way that light of a specific wavelength is scattered when they are illuminated by white light. This behavior results in the appearance of different colors in the LC as its temperature changes. When a thin coating is applied to an object, the colors of the LC's can be interpreted as surface temperatures on the object.

Compared to infrared thermography, liquid crystals have the disadvantage that they "operate" at a fixed temperature range; i.e., the thermal response of a given compound is constant. Also the specific level at which an indication appears is not variable for a given LC material. However, LC's are available in many types covering all useful temperatures and in temperature ranges from 3 to 15^{o}C. Also, LC's possess the major advantages that they are easy to use and inexpensive compared to the SIRC.

Thermography in its many forms has found application in a diverse number of areas. Substantial work has been done using SIRC's in medical applications, particularly cardiovascular and cancer studies. Recently,

concern over energy conservation has prompted extensive efforts to use thermography for locating poorly insulated areas of buildings and storage tanks. Some of these efforts have involved fly-over sensing of large residential areas, while others have used SIRC's in mobile vans to image single buildings. Other uses include quality assurance of electronic circuits, windshield testing and locating contraband at border check stations. However, not until the mid-1970's did thermography begin to receive much attention as a material testing technique. Since then, several studies have been made using both electronic and chemical imaging. The collective result of these studies indicated that thermography has a definite role in future material studies, but that further development must be done to make thermography more attractive for full-scale use. The efforts of the present study are directed toward this need.

Thermal Material Testing

One may classify thermal material testing techniques as either: (1) active, or (2) passive, according to how the thermal field is generated. In the active case, the material itself provides the heat necessary to generate a detectable surface temperature distribution. This is accomplished by placing the material under some form of cyclic strain, either by loading it in fatigue or by vibrating the part. Heat is then generated due to hysteresis effects in the material. This hysteresis heat generation is a function of stress level in the material (as well as cyclic frequency and material

compliance), so regions of high stress (such as geometric discontinuities and flaws) are accompanied by relatively high heat generation. Through the processes of conduction, convection and radiation, a temperature distribution is established in the material which is indicative of the material stress state. By thermographically visualizing this temperature distribution, one can locate damage regions within the material and/or conclude where the critical regions of the part are located. This active method of testing has been successfully demonstrated for both metals and composites in the recent past.

Generally, active testing has an advantage over passive testing in that the loading can be performed identically to that expected in service. Also, very subtle differences (such as between two seemingly identical geometric stress concentrations) can be evaluated using active techniques. However, the need to load the material may actually produce flaws in the part rather than detecting them, defeating the purpose of NDT. Active testing in-service might also require removal of a part from an assembly to allow high-frequency loading in a test fixture. In light of these problems, passive NDT becomes more attractive.

In passive thermal testing, heat is applied to the material from an external source and allowed to conduct throughout the material while the surface temperatures are monitored. Defects which may be present in the material serve to restrict the conduction of heat locally, creating detectable perturbations in the surface temperature field on the material. The size and type of the flaw determines its

effect on the surface field. Also, for the passive test to be successful, the flow of heat must be normal to the defect. In the case of an in-plane delamination of a composite, therefore, the heat must flow from back to front in order for the defect to be visualized. To detect a through-thickness crack, however, heat must be applied to the end of the part and allowed to flow past the crack. Limits on the resolving power of this type of test are determined by the material thermal properties, the heat source characteristics, and the imaging system used. One major difference between active and passive should be noted. Although it is sometimes possible to obtain transient thermal behavior during active tests, the temperature fields which are developed are most often steady-state, or at least very slowly changing. In comparison, passive tests are usually rapid-changing, transient phenomena in which the crucial image appears and then dissipates in a very short time (on the order of a few seconds at most). This observation has important implications in developing the technique used in this study for passive thermal NDT of composites.

Study Objectives

The primary goal of this study was to assess the potential of liquid crystal thermography for flaw detection in composites using passive heating techniques. In achieving this goal, several objectives were identified and realized. These were to:

(1) Develop techniques for heating the test specimens uniformly, applying the liquid crystals evenly, and recording the data (images) on color film.

(2) Derive and verify an analytical model describing the heat transfer in the flawed composite during the passive test.

(3) Use the model and experiments to identify the important variables in passive thermal tests and their effect on resolution.

(4) Perform passive thermal NDT of implanted defects and adhesive joint defects in several composite material systems.

Tests were performed on graphite/epoxy (G/E), fiberglass/epoxy (FG/E), and HMC/G/E sandwich materials. It was found that all but the smallest of defects could readily be "seen" using a LC imaging system. Using the numerical model developed it was determined that even smaller defects could be visualized by increasing the thermal input to the specimens. The effects of other parameters such as flaw size, flaw depth and mode of heating were also ascertained. These results will be discussed in a later section of this report.

An important and very successful technique developed was that of photographically recording the test results. Since the thermal images on the specimens appeared and dissipated so rapidly, ordinary photography was found to be insufficient to "capture" the best images on the specimens during the tests. It was found that the use of a motor drive unit on a 35 mm SLR camera could dependably record critical images in all cases, avoiding the use of a much more expensive high-speed motion picture recording format.

As a result of the many tests which were performed, the large amount of computer time used, and the large number of color slides taken, it can be concluded that passive LC thermography has a very high potential indeed for use in flaw detection of composites. Its high speed, low cost and relative ease of use should make it very attractive for use in manufacturing and quality assurance applications.

EXPERIMENTAL PROGRAM

An experimental program was devised to study passive thermal testing of composites in keeping with the objectives stated previously. In this program, specimens of fiberglass/epoxy and graphite/epoxy with implanted TFE "defects" were heated radiantly while their surface temperature fields were monitored with various LC compounds. Critical images were recorded photographically, and in almost all cases clearly indicated the location and extent of the implants. As a corollary study, three adhesive joint types were studied in the same manner, yielding images of bond defects and in some cases natural material defects. More details on the experimental apparatus, materials, and techniques used are given in the following sections.

Apparatus

In any material study using passive thermography, the two most important considerations are the heat source and the thermal imaging system. Secondary concerns are the means of recording images, measuring absolute temperatures and timing transient events.

It was decided after some initial investigation to use a radiant heat source to produce the temperature fields on the specimens. It is felt that radiant heating is desirable compared to contact heating

because the radiant input to the surface is usually more uniform. The uniformity of the heat input is critical to the successful imaging of flaws. Therefore, a special radiant heater was built, utilizing 8 standard light bulbs in a narrow but deep enclosure (see Figure 1). The enclosure walls were lined with aluminum to reflect the heat to the specimen, which was held in place by retaining clips. The opening of the enclosure was masked (except where the specimen was held) to allow viewing and photographing the specimen images without interference from the visible light from the bulbs. Power to the bulbs was controlled through a Variac, and by using the controller and selecting different wattage light bulbs, it was possible to obtain a wide range of radiant heat inputs to the material system. This relatively simple and unsophisticated system provided a variable intensity, uniform thermal input for all the configurations tested.

Liquid crystals (LC's) are available in several forms, including encapsulated sheets, black-filled pastes, and pre-mixed liquids. It was decided, based on previous experience, to use the pre-mixed liquid form (available from Pressure Chemical Company, Pittsburgh, Pennsylvania) in several temperature levels. Any LC has both a temperature "level" and a temperature "range." The level usually refers to the temperature at which the crystals begin to indicate (e.g., $24^{\circ}C$). The range indicates over what span of temperatures the crystals continue to indicate ($3^{\circ}C$ in this case). Thus, using

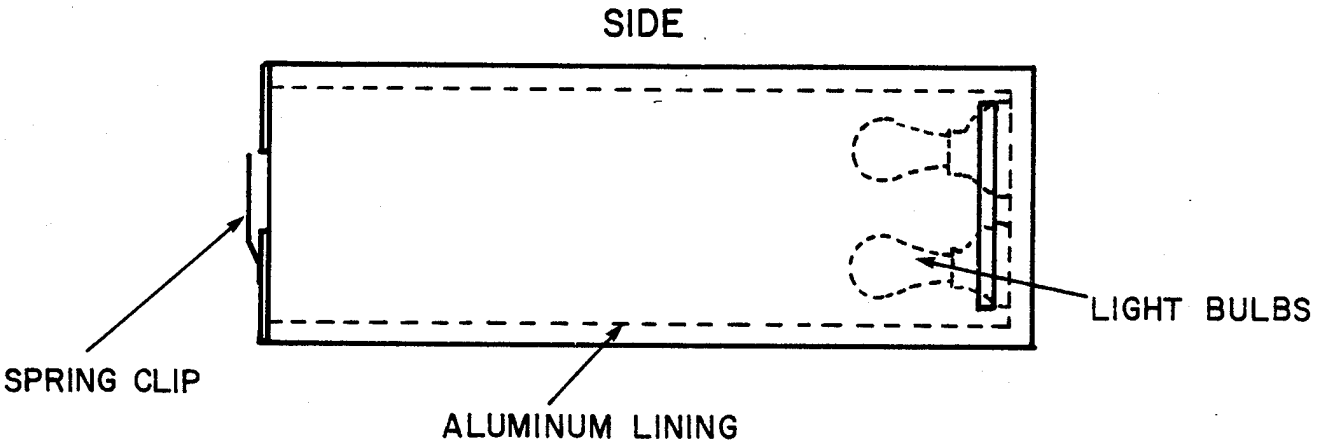

FIGURE 1. RADIANT HEAT SOURCE

the nomenclature for the LC's employed in this study, LC-124 begins to indicate at 24°C and continues until 27°C, having a range of 3°C. The indications proceed from red at 24°C, through yellow and green, to blue at 27°C. At temperatures below 24°C and above 27°C, the crystals are clear. Three different LC compounds were used in this study: LC-124, LC-127, and LC-130. The temperature ranges and levels for these specified by the manufacturer were only approximate, and a calibration check was performed to determine actual response.

The method of applying a given LC to a test specimen is critical to the success of the tests, since an uneven coating can produce false images and mask true ones. In this study, the LC's were carefully sprayed on prepared specimens using a artists' airbrush. This produced a consistently uniform coating and was to a large degree responsible for the high quality of the results.

The specimens were prepared by cleaning them and painting them flat black. Since LC's scatter certain wavelengths of incident light, a black coating is necessary to absorb all non-scattered light, improving the color rendition of the LC's. (By using non-soluble paint and LC's, it is possible to apply one under coat of paint and several LC applications, washing the specimen with LC solvent between applications.)

A technique for recording the images photographically was developed which proved to be very successful. Since the images from LC's are in colors, it is necessary to use color photography to record them. In this study, Kodak Ektachrome slide film (balanced for tungsten light)

was used in a Canon F-1 SLR camera. The film was push-processed to ASA 320 (twice its normal speed) to avoid long exposures. The specimen was illuminated with two 100 w. bulbs only during exposures (to minimize heat input from these bulbs). Since the images in some cases were so transient, it was necessary to utilize a Motor Drive unit on the camera to reliably capture the best indications. This unit allowed either single exposures or multiple exposures at about 3.5 frames per second. The system thus used provided excellent records of results without necessitating the use of more expensive color motion picture systems.

In order to also record time information with the LC images, a special timer was constructed for use with the camera. This timer displays elapsed time up to 9999.99 seconds. The digital display is in 0.5-inch LED's. The timer was to be simply placed in the field of view of the camera during exposure. However, since the required exposure was 1/15 sec, it was necessary to "freeze" the display during the exposure to avoid blurring the last two digits. To do this, a latch was designed into the circuit, to be triggered by the camera's flash synchronization jack. During the exposure, the display was frozen while the elapsed time continued correctly. After each exposure, the display returned to count the correct elapsed time. In this manner, an accurate record of time was included in each of the data records made.

Finally, in some cases, independent quantitative temperature measurements were desired. Two methods of measuring temperature were used. In one method, a digital thermometer with thermistor probes was used (Cole-Parmer Model 8502-25). The probes were used to measure air temperature, or overall specimen temperature (when taped to the specimen). The second method employed bondable foil temperature gages (Micro Measurements ETG-50B) on the surfaces of the specimens. These gages, in conjunction with an x-y recorder with a time-base, yielded records of transient temperature rise on the front and back surfaces of graphite/epoxy and fiberglass/epoxy specimens. These records were used to help verify the analytical model developed.

In performing a test, the equipment described was set up as shown in Figure 2. The prepared and coated specimen was allowed to come to thermal equilibrium in the test room, and then was placed in the heat source. The heat was applied rapidly, while the elapsed timer was simultaneously started. As the thermal image became visible, a series of exposures were made with the camera. For most cases, the actual test took only a few seconds.

Materials Studied

In this program, three material systems were studied: (1) graphite/epoxy (G/E), (2) fiberglass/epoxy (FG/E), and (3) a sandwich plate of high-density molding compound (HMC) and G/E.

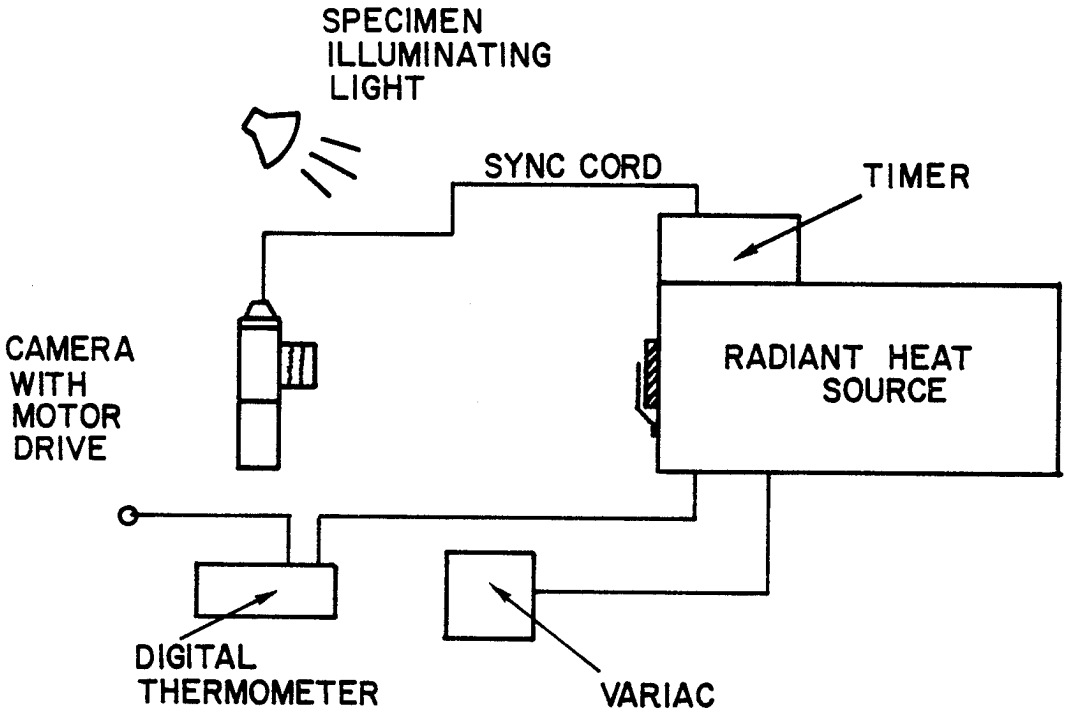

FIGURE 2. EXPERIMENTAL SET-UP

Three different types of G/E specimens were fabricated. A large number of specimens were made with two implanted "defects" at their midplane. These specimens of 8, 16, and 24 plies were made from AS/3501-6 graphite prepreg {ply thickness = .0055 in (0.140 mm)} using a quasi-isotropic layup, $(0^{\circ}/\pm 45^{\circ}/90^{\circ})_{ns}$. They were made using standard fabrication techniques and autoclave cure cycles. The "defects" were simulated by circular TFE disks {.001 (.0025 mm) thick} implanted during processing. One location received one disk while the other had a double-thickness, or two disk, defect. The disks ranged in size from 0.10" to 0.50" diameter. The finished specimens were 1.50" (38.1 mm) wide and approximately 12.00" (30.4 cm) long.

A similar G/E specimen was made for each defect size, but several implants were made at different depths in the specimen. These specimens were used to study the effect of flaw depth on the image quality.

The final G/E specimen fabricated was a large {3.00" (76.2 mm) x 12" (45.72 cm)} 8-ply plate of unidirectional 0° layup. This plate contained nine separate defects in the forms of circles, squares, triangles, and rectangles. This specimen was used to investigate the ability of thermal imaging to resolve special shapes and indicate them as such.

One special fiberglass/epoxy specimen was fabricated to include implanted circular defects of 0.10", 0.20", 0.30" and 0.40" (2.54 mm, 5.08 mm, 7.62 mm, 10.16 mm) diameter. This laminate was an 8-ply

unidirectional (0^{o}) plate made from 1002 E-glass/epoxy prepreg {ply thickness = .0085" (.216 mm)} using standard fabrication techniques. The defects were spaced evenly along the centerline of the specimen at its mid-plane.

In a related effort, bond defects in adhesive joints were studied. Panels of graphite/epoxy were bonded together with Eccobond 45 (room-temperature setting epoxy). Over part of the bond area, voids in the adhesive were purposely created, while over the remaining part, a perfect bond was sought. Similarly, an adhesive joint specimen was made using fiberglass/epoxy panels.

Finally, an industrially-supplied sandwich plate was tested, since its surface exhibited bubbles or signs of debonding between the faces and core. The faces were each two plies of G/E (0^{o}, 90^{o}), which were co-cured with the core of high-density molding compound (HMC). The HMC core was later found to contain numerous delaminations. It should be noted that the HMC core does not use an epoxy matrix, but rather a polyester one.

As a basis for comparison, each of the specimens was tested for implanted or other defects using C-scan ultrasonic techniques. All of the defects could be verified, with the notable exception of the HMC material, where large delaminations could not be found using the C-scan. For reference, all of the specimen C-scans are included in Appendix A of this report.

EXPERIMENTAL RESULTS

A summary of the experimental results of this program is given in Table 1. This table shows specimen configuration, defect size, imaging systems used, and whether the defects could be imaged.

To include all of the thermograms made during this study in this report would be impossible, since over 1200 slides were taken. Instead a number of the representative color slides have been reproduced in black and white for inclusion herein. These figures show each material system used and most of the defect configurations. The reader may wish to refer to the appendix for C-scans of each specimen shown.

The results qualitatively assess the resolution of the three LC imaging systems for the material systems defect types and laminate configurations discussed. Images of the defects ranged from diffuse to sharp depending upon the combination of laminate thickness, heat input and LC system used. The general geometry of defect was perceptable even for the diffuse images.

The test program described in Table I summarizes the results of the study in terms of observed defects. It does not indicate the clarity of the observed image or describe the test conditions. The following discussion of results will treat this in more detail.

TABLE 1 SUMMARY TEST PROGRAM AND RESULTS

Material	Laminate Configuration	Defect Type	Defect Geometry	Flaw Sizes Detected (in)/mm					LC System
				0.1/	0.2/	0.3/	0.4/	0.5/	
Gr/E	$(0/\pm45/90)_{25}$	TFE(S)	Disk	x	x	x	x	x	LC 124
Gr/E	$(0/\pm45/90)_{25}$	TFE(D)	Disk	x	x	x	x	x	LC 124
Gr/E	$(0/\pm45/90)_{25}$	TFE(S)	Disk	x	x	x	x	x	LC 127
Gr/E	$(0/\pm45/90)_{25}$	TFE(D)	Disk	x	x	x	x	x	LC 127
Gr/E	$(0/\pm45/90)_{25}$	TFE(S)	Disk	x	x	x	x	x	LC 130
Gr/E	$(0/\pm45/90)_{25}$	TFE(D)	Disk	x	x	x	x	x	LC 130
Gr/E	$(0/\pm45/90)_{35}$	TFE(S)	Disk		x	x	x	x	LC 124
Gr/E	$(0/\pm45/90)_{35}$	TFE(D)	Disk		x	x	x	x	LC 124
Gr/E	$(0/\pm45/90)_{35}$	TFE(S)	Disk		x	x	x	x	LC 127
Gr/E	$(0/\pm45/90)_{35}$	TFE(D)	Disk		x	x	x	x	LC 127
Gr/E	$(0/\pm45/90)_{35}$	TFE(S)	Disk		x	x	x	x	LC 130
Gr/E	$(0/\pm45/90)_{35}$	TFE(D)	Disk		x	x	x	x	LC 130
Gr/E	$(0/\pm45/90)_{45}$	TFE(S)	Disk		x	x	x	x	LC 124
Gr/E	$(0/\pm45/90)_{45}$	TFE(D)	Disk		x	x	x	x	LC 124
Gr/E	$(0/\pm45/90)_{45}$	TFE(S)	Disk		x	x	x	x	LC 127
Gr/E	$(0/\pm45/90)_{45}$	TFE(D)	Disk		x	x	x	x	LC 127
Gr/E	$(0/\pm45/90)_{45}$	TFE(S)	Disk		x	x	x	x	LC 130
Gr/E	$(0/\pm45/90)_{45}$	TFE(D)	Disk		x	x	x	x	LC 130
Glass/E	$(0)_8$	TFE(D)	Disk	x	x	x	x	x	LC 124
Glass/E	$(0)_8$	TFE(D)	Disk	x	x	x	x	x	LC 127
Glass/E	$(0)_8$	TFE(D)	Disk	x	x	x	x	x	LC 130

TABLE 1 (CONTINUED)

Material	Laminate Configuration	Defect Type	Defect Geometry	Flaw Sizes Detected (in)/mm					LC System
				0.1/	0.2/	0.3/	0.4/	0.5/	
Gr/E	$(0)_8$	TFE(D)	MD*	x	x	x	x	x	LC 124
Gr/E	$(0)_8$	TFE(D)	MD*	x	x	x	x	x	LC 130
Gr/E	$(0)_8$	Disbonded	N.A.			Flaws Detected			LC 124
Glass/E		Disbond	N.A.			Flaws Detected			LC 124
Gr/E/HMC	(0/90/HMC/90/8)	Delamination	N.A.			Flaws Detected			LC 124
GR/E	$(0/\pm45/90)_{45}$	Stepped TFE	Disk			x			
GR/E	$(0/\pm45/90)_{45}$	Stepped	Disk			x			

Initially the intensity of the heat source and its effect on imaging had to be measured. Three levels of heat input were evaluated and the results qualitatively showed a relationship between the intensity of the heat input and image clarity. Increasing the heat input intensity improved the image definition while shortening the image first indication time and duration. These results correlate with the parametric studies conducted using the finite difference model. The largest radiative heat input was used for all subsequent studies.

Graphite/epoxy specimens with single and double feflon (TFE) implanted defects ranging in size from 0.1 in (2.54 mm) to 0.5 in (12.7 mm) were used to measure the resolution of the imaging system. Attempts were made to detect these flaws at the midplane of 8, 16 and 24 ply quasi-isotropic laminates with each of the three LC systems. In the 8 ply (.044 in/1.12 mm) laminate all of the defects were detected. Double-thickness defects appeared sharper than single-ply defects, indicating that thermal imaging of defects is very sensitive to small changes in thermal conductivity caused by defects. Although the defects could be imaged by all three LC systems the LC124 system gave the clearest images. The apparent reason for this will be discussed later.

The 0.1 in (2.54 mm) defects could not be clearly imaged in the 16 and 24 ply graphite/epoxy specimens but all of the larger defects could be seen. A pronounced decrease in image clarity was noted in the thicker laminates, as shown in Figures 3-5. Those figures show black and white reproductions of 0.3 in (7.62 mm) defects (single and double ply TFE) in 8, 16 and 24 ply laminates; respectively, as imaged

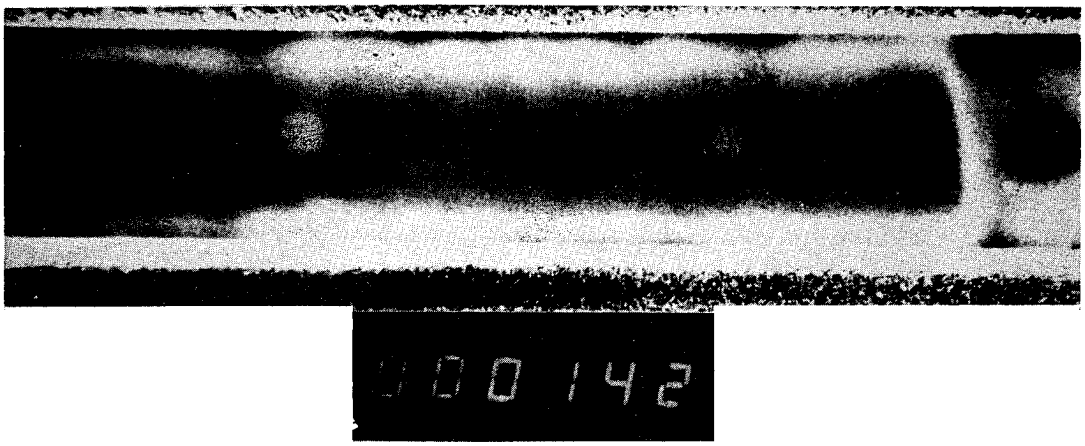

FIGURE 3. LC 124 IMAGING COMPOUND ON AN 8 PLY $[0/\pm45/90]_s$ LAMINATE.

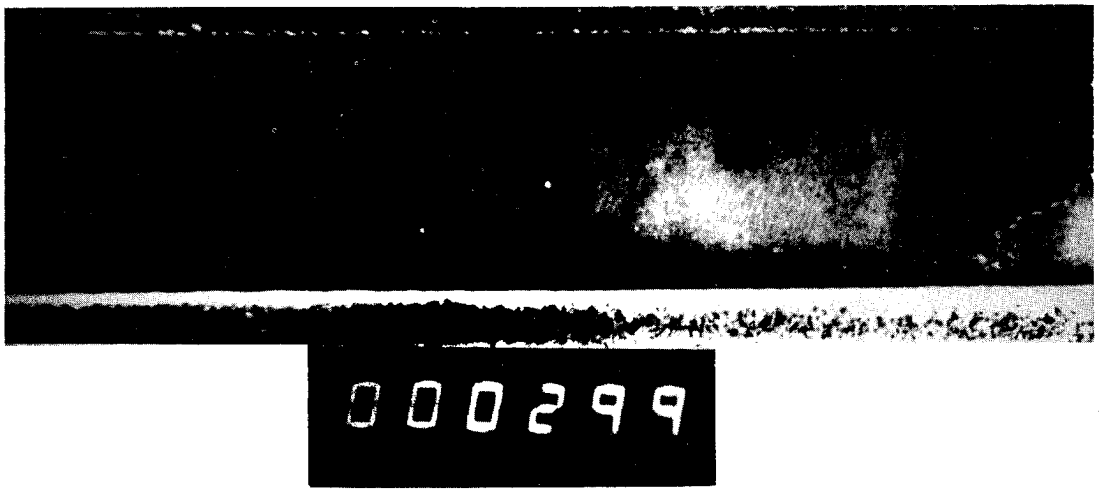

FIGURE 4. LC 124 IMAGING COMPOUND ON A 16 PLY $[0/\pm45/90]_{2s}$ LAMINATE.

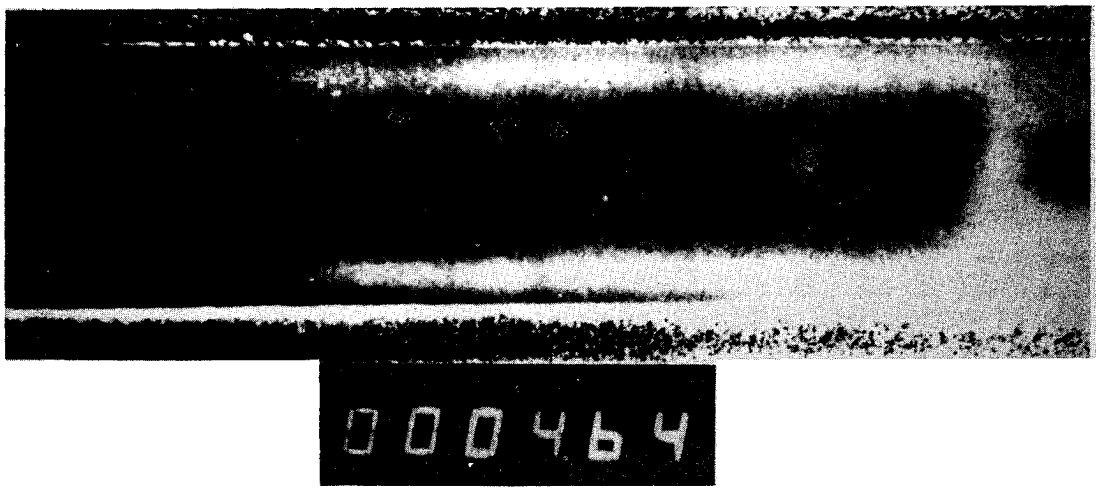

FIGURE 5. LC 124 IMAGING COMPOUND ON A 24 $[0/\pm45/90]_{3s}$ LAMINATE.

by the LC 124 liquid crystal system. Notice that the times to the first indication are linearly increasing with thickness indicating that the heat input intensity was constant for each case. Results from a carefully controlled set of experiments are summarized in Figure 6, verifying the linearity of first indication time as a function of laminate thickness. The significance of these results becomes apparent when coupled with information from the parametric studies. The decreasing clarity of the defect image with increasing thickness implies a relationship between heat input, material thickness, material thermal properties and its effect on the temperature gradients observed at the surface. This is studied by the finite difference heat conduction model in more detail.

A Fiberglass/epoxy laminate was similarly used to evaluate the resolving power of the technique in a material with lower thermal conductivity. Tests conducted on a 16-ply laminate revealed that the heat source was not large enough to cause a clear indication. Results from tests on an 8-ply glass/epoxy laminate with an array of double thickness TFE defects ranging in size from 0.1 in (2.54 mm) to 0.4 in (10.16 mm) are shown in Figure 7. Though the black on white reproduction is not as clear as the color original, all of the defects are clearly visible. Again the LC 124 system gave the best results but the other two systems worked satisfactorily.

Two important results were obtained from tests conducted on the unidirectional graphite/epoxy sample containing defects with square, triangular, circular and rectangular geometries. The geometry of

FIGURE 6. FIRST INDICATION TIME AS A FUNCTION OF SPECIMEN THICKNESS FOR GR/E QUASI - ISOTROPIC LAMINATE.

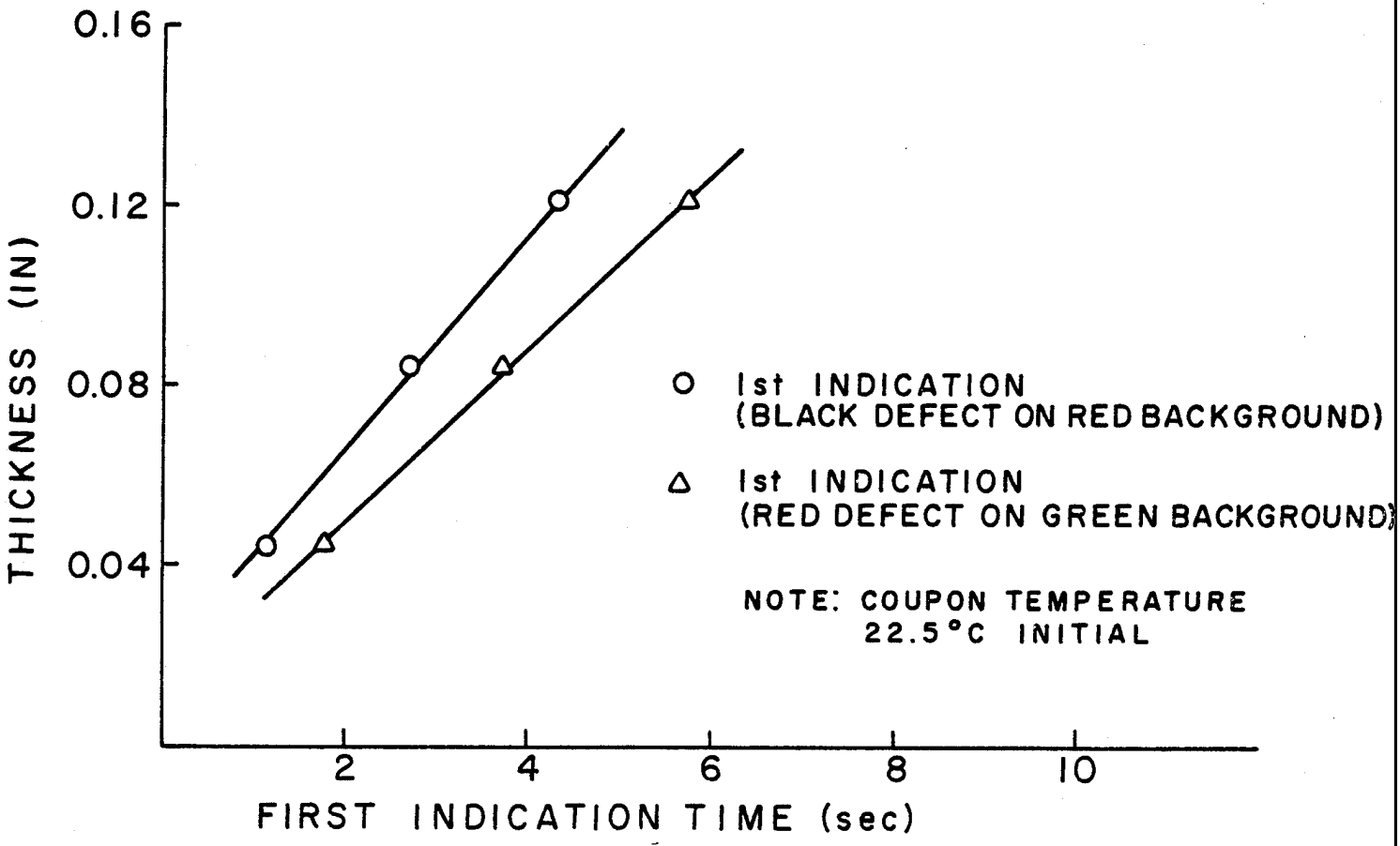

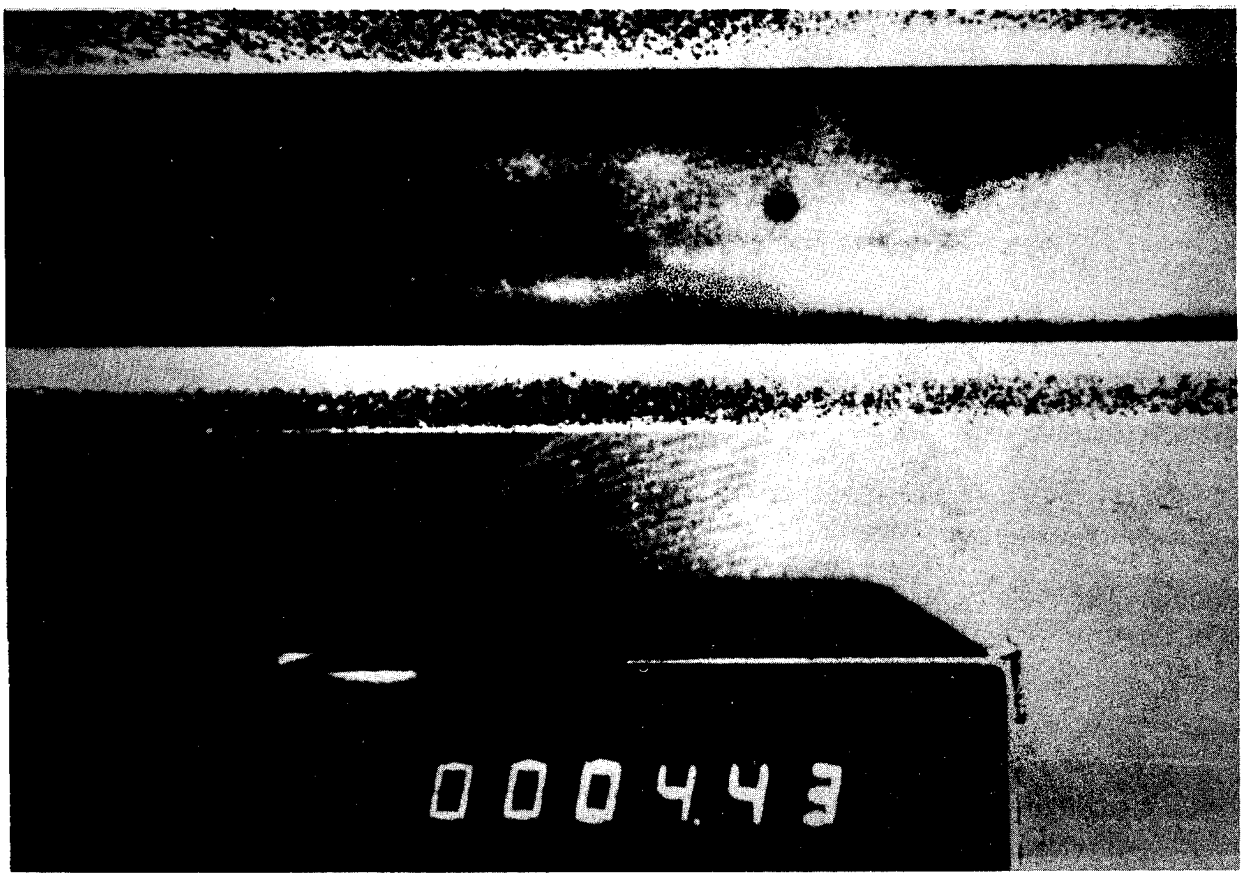

FIGURE 7. LIQUID CRYSTAL IMAGE OF 4 INTERLAMINAR TEFLON IMPLANTED FLAWS RANGING IN SIZE FROM 0.4 in. (10.2 mm) TO 0.1 in. (2.5 mm) DETECTED IN AN 8 PLY 0° GLASS/EPOXY LAMINATE.

the defect is captured in the thermographic image as is apparent in Figure 8. The two images depicted in the thermograms in Figure 8 occurred 0.3 seconds apart. The fibers were oriented horizontally across the specimen. This sequence illustrates the importance of the anisotropic nature of the material in affecting the defect image. High conductivity in the fiber direction causes the image to "wash out" or neck down along the fibers dramatically, as seen for the vertical rectangles, while the horizontal rectangles are not as drastically affected.

A graphite/epoxy laminate was fabricated with 0.3 in (7.62 mm) defects stepped through the thickness to assess the effect of flaw depth on image resolution. The defects could all be imaged, but the clarity was not equal for all defects. Defects located nearest the back surface produced more diffuse images than those located near the front surface. Results were similar for each of the three LC systems. The laminate used in this experiment was 24 plies thick and thus was not loaded with optimum heat input, as previously discussed.

Detection of bond imperfections in lap joints was assessed by fabricating voids in the bond lines of joints in two material systems, gr/E and glass/E . Excellent results were obtained for both materials as illustrated in the thermograms in Figures 9 and 10. Figure 9 shows the gr/E joint. Arrows indicate the suspected flaws. Sections taken through the flawed regions verified all of the indicated flaws. Figure 10 is a thermogram of the glass/E joint with

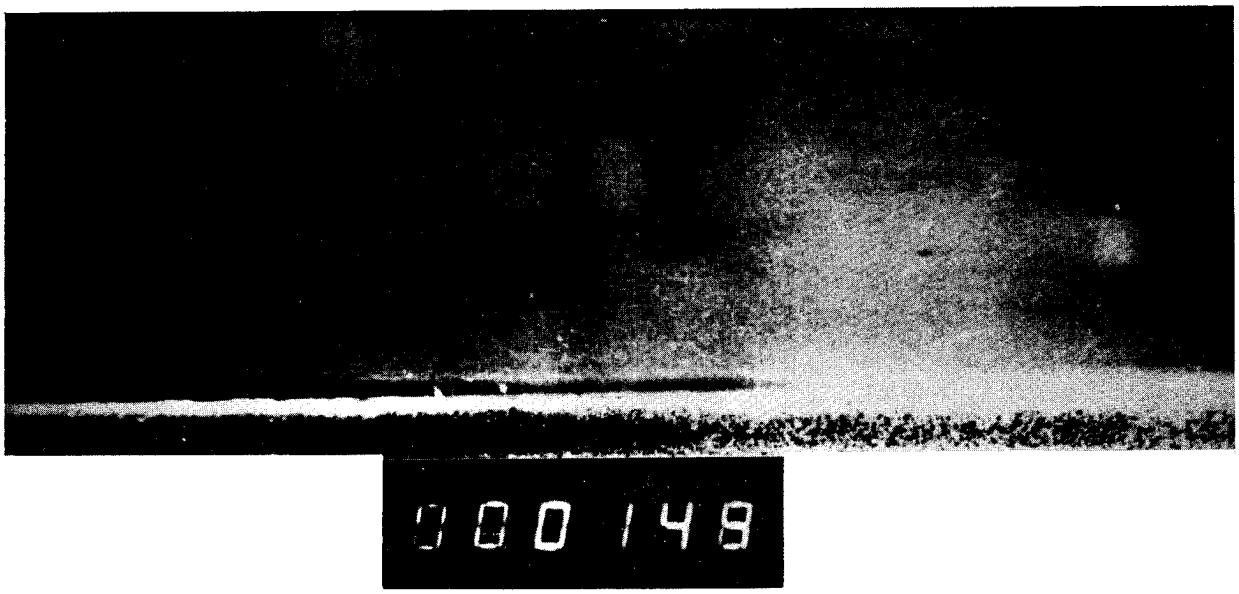

FIGURE 8a. THERMOGRAPH OF IMPLANTED FLAWS POSSESSING DIFFERENT GEOMETRIES AS IMAGED IN A UNIDIRECTIONAL 8 PLY GRAPHITE/EPOXY LAMINATE.

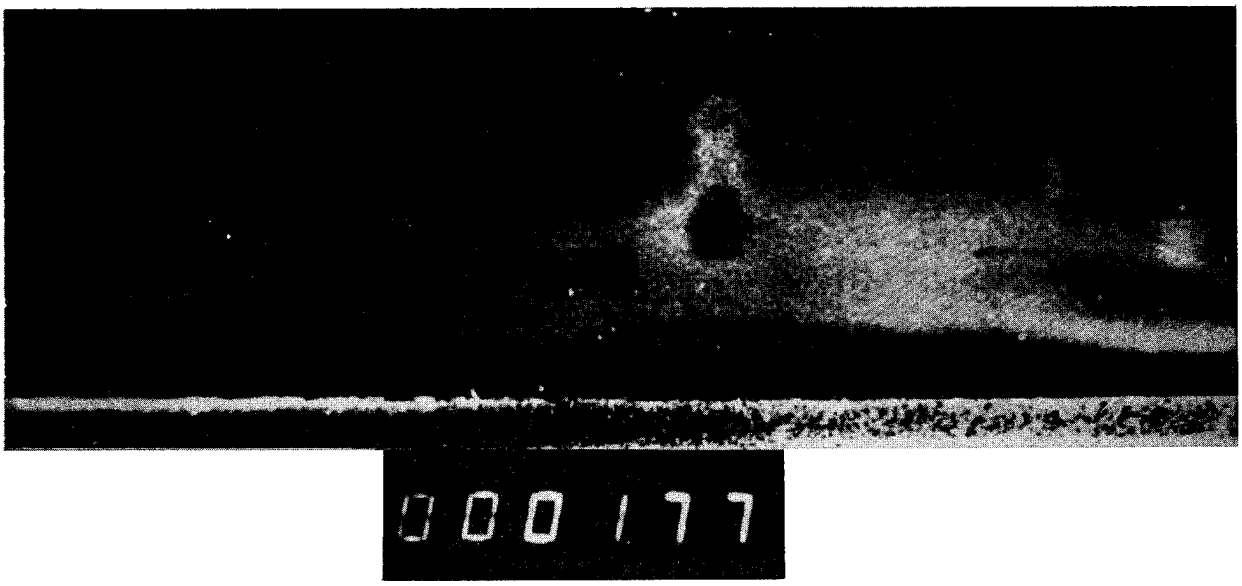

FIGURE 8b. SAME THERMOGRAPH SHOWN ABOVE, ONLY 0.3 SECONDS LATER.

THERMOGRAM

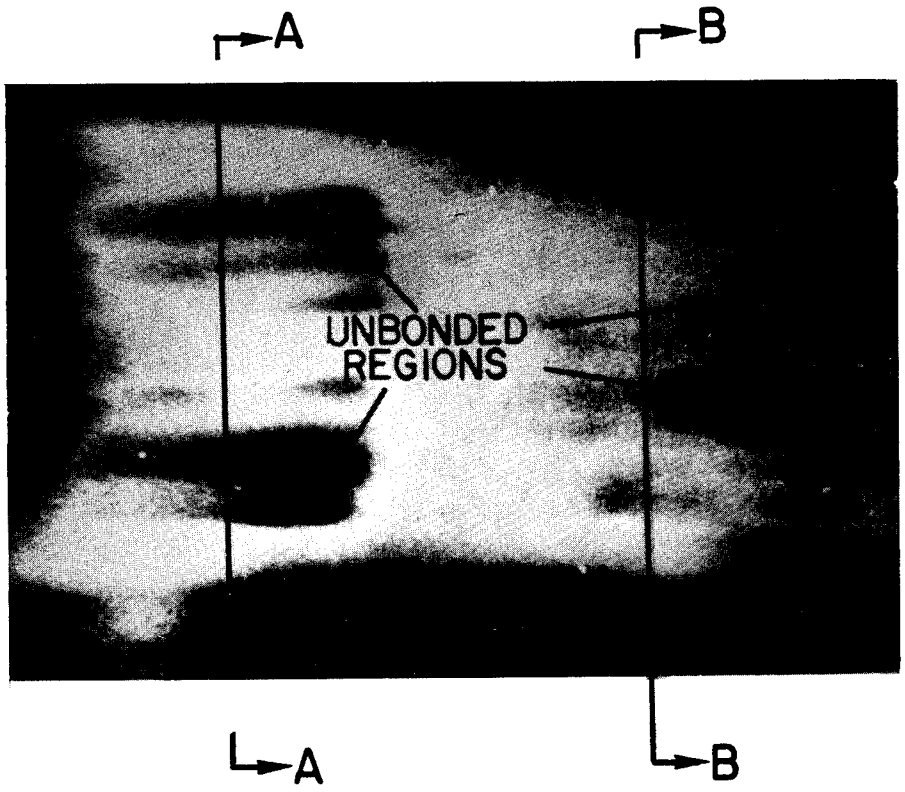

ULTRASONIC C-SCAN

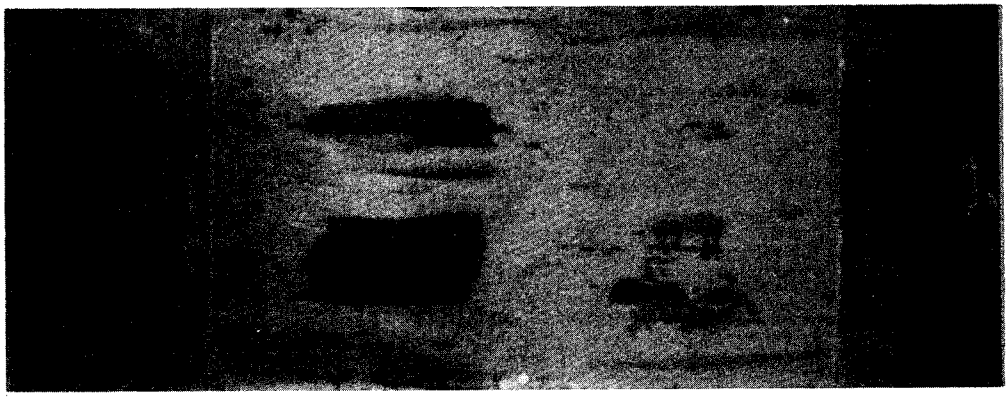

FIGURE 9a. GRAPHITE/EPOXY BONDED JOINT

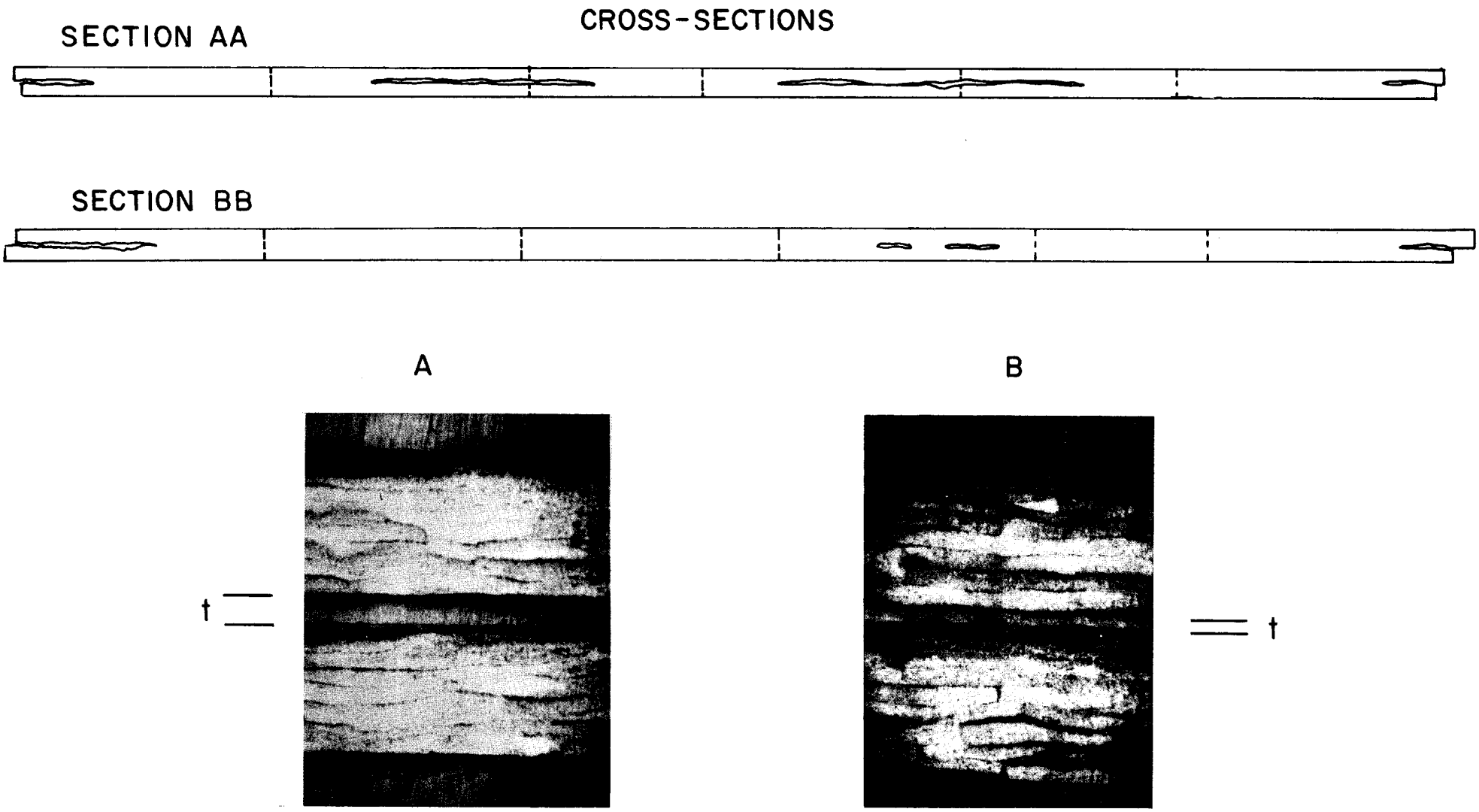

FIGURE 9b.

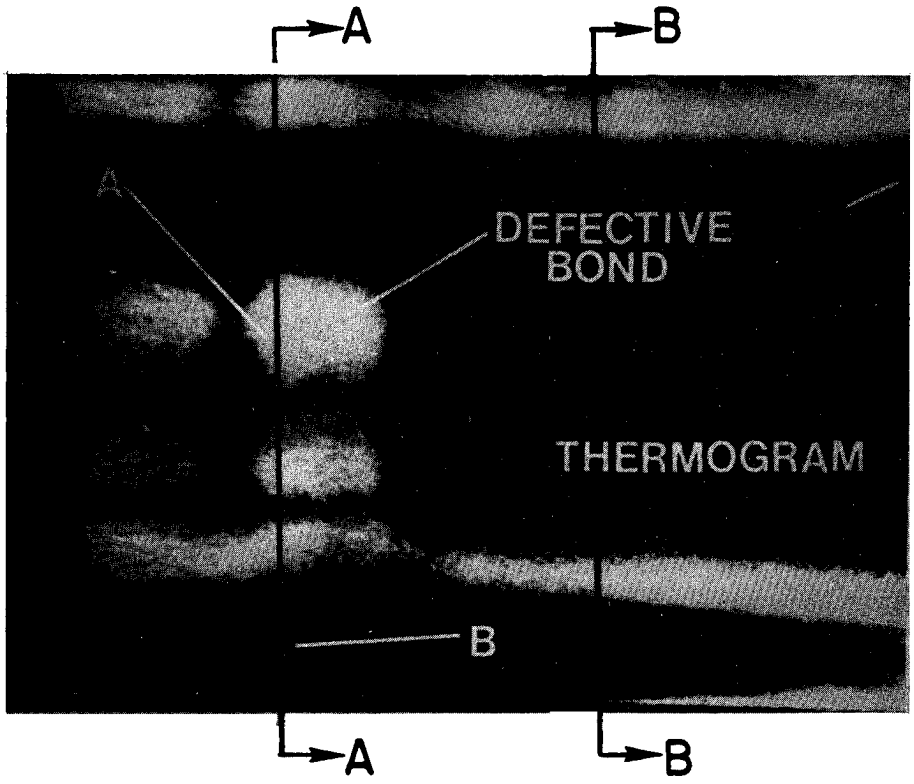

ULTRASONIC C-SCAN

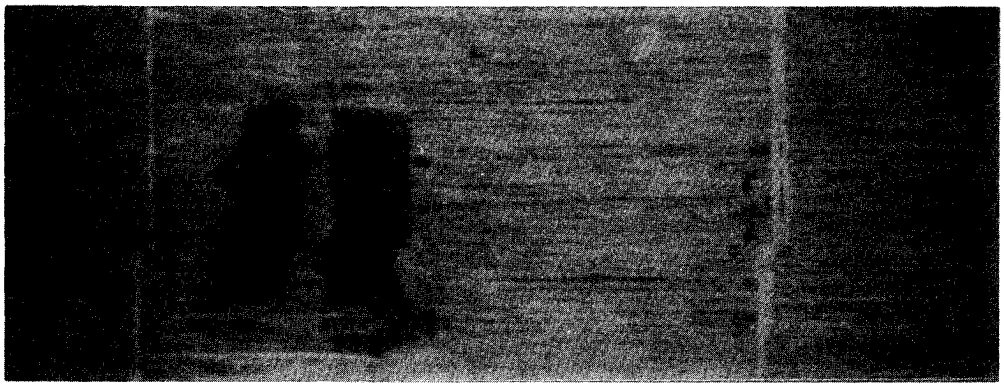

FIGURE 10a. GLASS/EPOXY BONDED JOINT.

CROSS-SECTIONS

SECTION AA

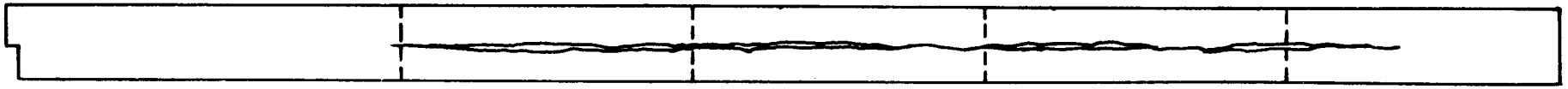

SECTION BB

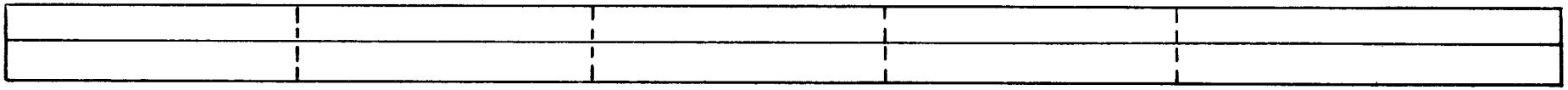

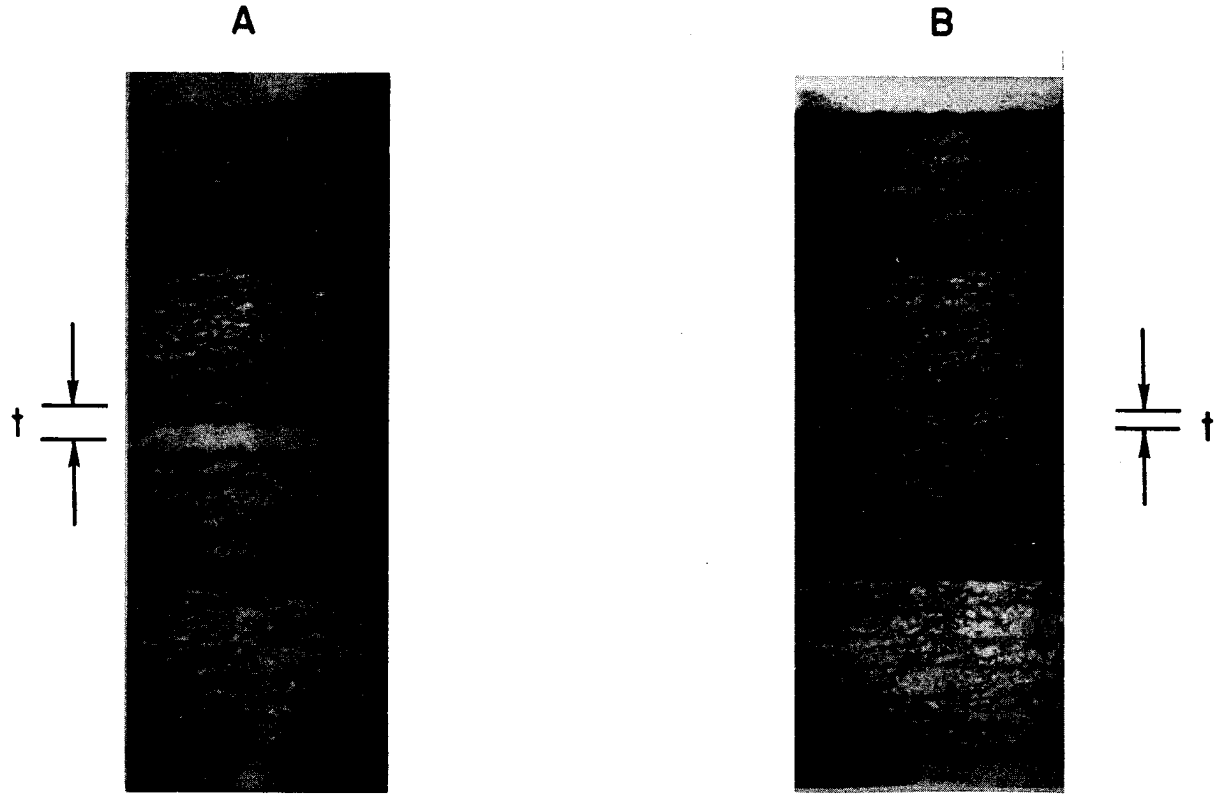

FIGURE 10b.

THERMOGRAM

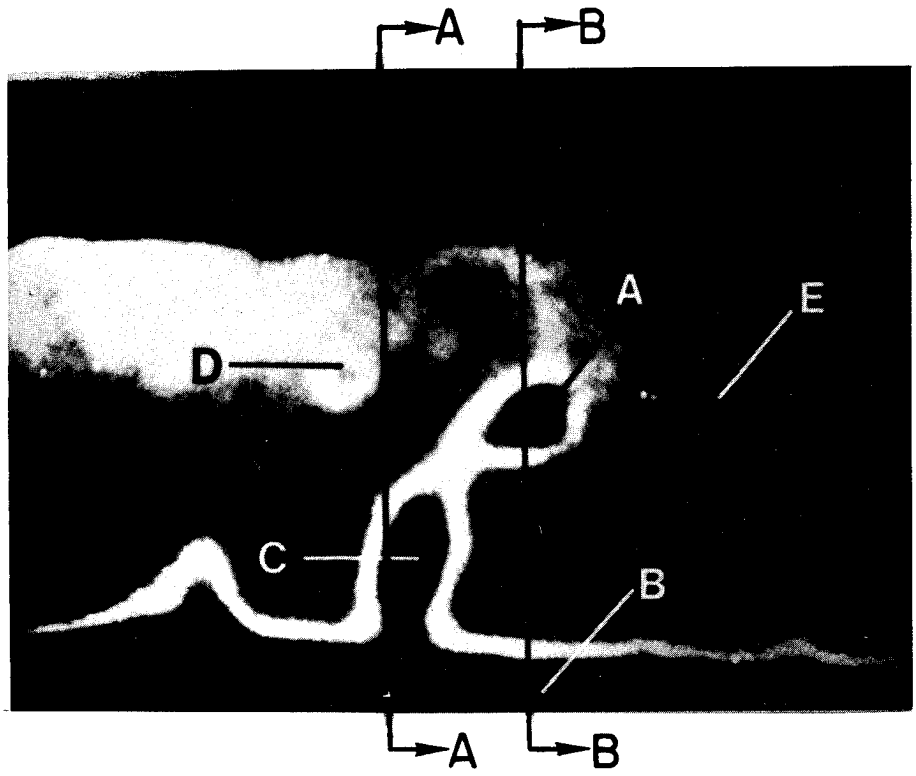

ULTRASONIC C-SCAN

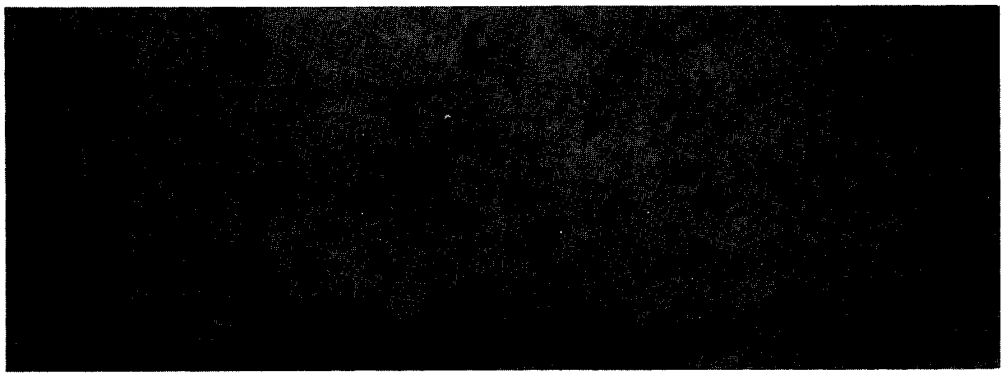

FIGURE IIa. HMC - GRAPHITE/EPOXY HYBRID MATERIAL

CROSS - SECTIONS

SECTION AA

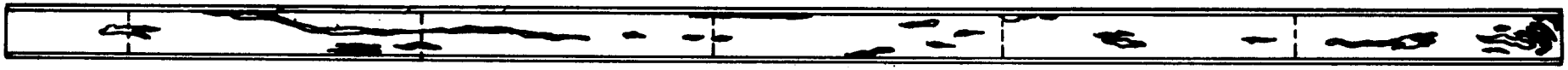

SECTION BB

PHOTOMICROGRAPHS

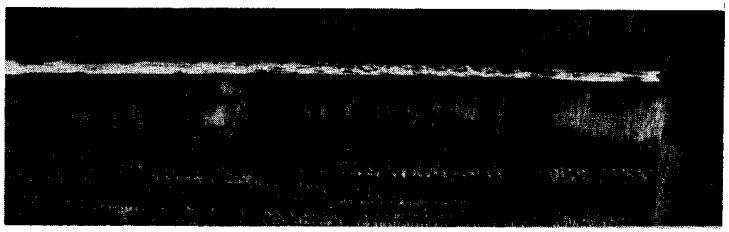

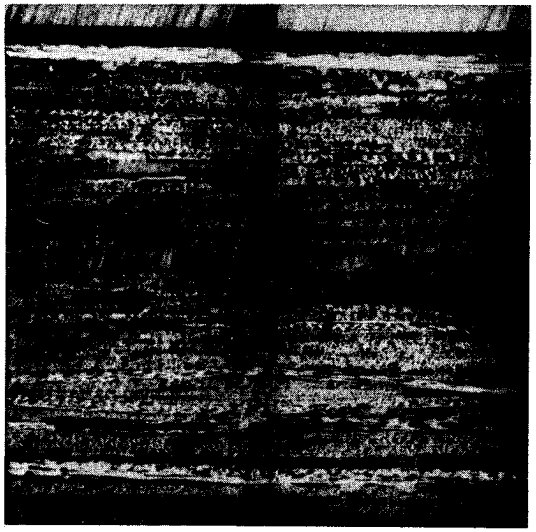

FIGURE 11b.

the flawed region again identified by the arrows. Sections were similarly taken from this joint and the flaws were verified. These results clearly suggest the utility of thermography in detection of flaws in adhesive joints. Comparison with the ultrasonic C-scans of these bonds shows the excellent correspondence between the two methods.

To test the ability of liquid crystals to image real defects (delaminations, voids, etc.) a piece of graphite/epoxy-HMC sandwich structure was tested. One of the resultant thermograms (Figure 11) shows numerous flaws. Sections were taken through suspicious regions of the panel and the findings are labeled in the figure. An ultrasonic inspection was performed on the laminate three times, using different gate settings, and the results were compared to the thermogram. Some of the defects correspond perfectly but the large delamination shown at location A on the thermogram was barely detectable by ultrasonic inspection. Two of the scans did not reveal anything, the third showed a very small region of delamination. The sectioning revealed a very large delamination located in the region indicated on the thermogram, but not defined by the C-scans.

The results from the studies performed on the gr/E laminates raised questions about the accuracy of the LC indication temperatures and ranges. A calibration was performed for each of the LC systems used and the results are in Figure 12. The liquid crystals systems are supposed to have ranges of $3^{o}C$ ($5.4^{o}F$) and first indication temperatures of $24.2^{o}C$ ($75.6^{o}F$), $27.2^{o}C$ ($81.0^{o}F$), and $30.2^{o}C$ ($86.4^{o}F$), respectively

FIGURE 12. CALIBRATION OF LIQUID CRYSTAL INDICATION TEMPERATURES.

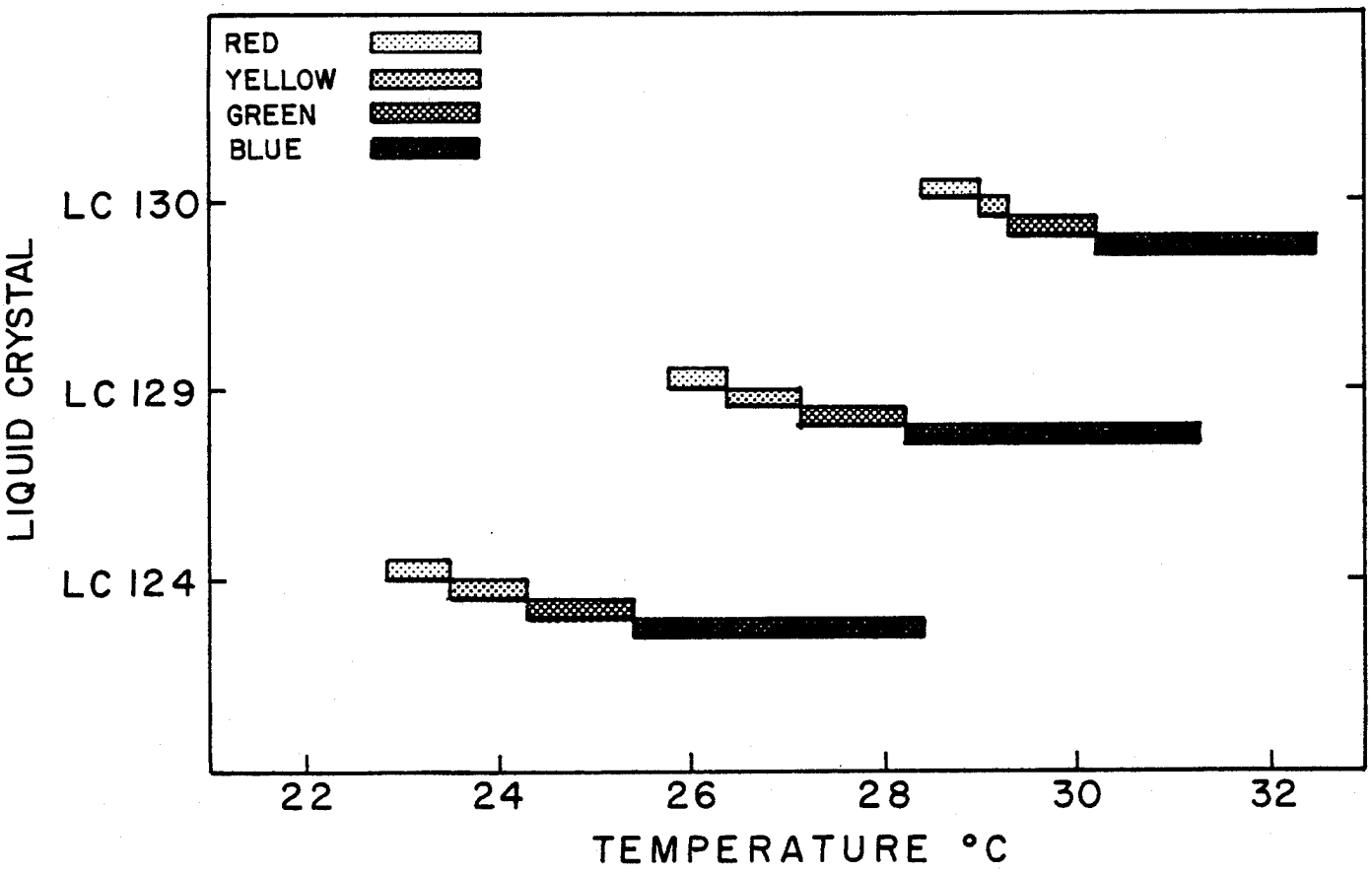

for the LC 124, LC 127 and LC 130 types. Significant variation from this data was observed. The indication ranges for each color were not constant. The blue indication consistently spanned a wider range of temperatures than the red indication. Typically the yellow indication range was narrow with green having the next widest range. Assessment of the results suggest that control of the indication ranges and first indication temperatures of liquid crystal systems could enhance image clarity. Therefore, accurate calibration of liquid crystal systems may become an important part of the thermographic technique.

ANALYTICAL MODEL AND RESULTS

To aid in the analysis of passive thermal NDT of composites, a theoretical model of the situation was developed. Due to the complexity of heat transfer in composites, and the transient nature of the passive tests, it was necessary to develop a numerical model and a computer program for the solution to the problem. This model was then used to perform a parametric study of passive NDT and identify the governing variables in the process.

Theory

The problem to be modeled involves the transient conduction of heat in a composite material heated from one surface. Furthermore, it was also desired in this study to model an in-plane defect somewhere in the composite. The problem was complicated by the anisotropic nature of heat conduction in composites. Finally, the result had to be in the form of a temperature field on the viewed surface of the specimen. From this field, one could calculate thermal gradients, which are important as a measure of the resolution of the defect.

It was determined that the most expedient approach to the problem would be through a finite difference solution to the governing differential equation:

$$\rho\, C_p \frac{\partial T}{\partial t} = k_x \frac{\partial^2 T}{\partial x^2} + k_y \frac{\partial^2 T}{\partial y^2} + k_z \frac{\partial^2 T}{\partial z^2} \qquad (1)$$

where ρ = net material density

C_p = net material specific heat

T = temperature

$k_{x,y,z}$ = thermal conductivity in x-, y-, and z-directions, respectively.

In the finite difference approach, the body is modeled by a matrix of nodes, each associated with a small volume of material. The governing equation is then written for each node, yielding a set of algebraic equations to be solved. For transient heat transfer problems, the solution may be formulated in either a "forward-differencing" format (moving forward in time, starting with initial conditions) or a "backward-differencing" format. The forward-differencing approach allows one to write the nodal equations for temperature at time $t+\Delta t$ in terms of the temperatures of all surrounding nodes and the considered node at time, t. This explicit formulation results in a somewhat simpler solution and was used in this study.

It was decided to try to model only a small section of the composite plate, namely the region just surrounding the defect. This was necessary because it was desired to model each individual ply, restricting the thickness of each nodal volume. This in turn leads to a reduction of the maximum allowable time increment for numerical stability. Hence, to model the entire plate would have required a prohibitively high number of nodal equations and solution iterations.

The use of a "small section" is acceptable if the defect does not perturb heat conduction near the edges of the section, which were assumed to be insulated. It was found that these boundary conditions are in fact reasonable for the cases studied here.

The remaining conditions imposed were insulated surfaces and a uniform, room-temperature initial condition. Of these two, the insulated surface is of questionable accuracy. For short-times (~ 1 sec), surface temperatures are low enough that the effects of convection and radiation from the surfaces are minimal. However, for longer times, this is not strictly correct, and a revision of the model should be made.

Now, assuming that it is satisfactory to model a section of the plate as described, it is necessary to write the finite difference equations for the nodes in the section. As mentioned, the need to individually model each ply complicates the analysis since the plies may have any orientation. It is, therefore, required to specify a global axis system for the section (x,y,z) and resolve the anisotropic thermal conductivity of each ply into this system. In order to analyze any 2-component material system, thermal properties are derived from the properties of the matrix and fiber materials. For density and specific heat, the Rule of Mixtures is used.

$$\rho = \rho_f V_f + \rho_m (1-V_f) \tag{2}$$

$$C_p = C_f V_f + C_m (1-V_f) \tag{3}$$

where V_f = volume fraction of fiber

$(\ )_m$ = matrix properties

$(\ )_f$ = fiber properties

Within each ply, the thermal conductivity in the longitudinal (fiber) direction (k_ℓ) and transverse directions (k_t) may be calculated:

$$k_\ell = k_f V_f + k_m(1-V_f) \tag{4}$$

$$k_t = k_m \left[\frac{k_f(1+V_f)+k_m(1-V_f)}{k_f(1-V_f)+k_m(1+V_f)}\right] \tag{5}$$

where k_f = fiber conductivity

k_m = matrix conductivity

Knowing these thermal conductivities, the global x,y, and z conductivities are easily obtained:

$$k_x = |k_\ell \cos\theta| + |k_t \sin\theta|$$

$$k_y = |k_\ell \sin\theta| + |k_t \cos\theta| \tag{6}$$

$$k_z = k_t$$

where θ = fiber orientation angle with respect to the global x-axis.

The properties to be used in the numerical model are those given in Equations (2), (3), and (6).

DESCRIPTION OF DEFECT

The approach described thus far will suffice for modeling an unflawed material, but in the present study an important part of the model addressed the simulation of a defect. It was assumed that a defect, either natural or implanted, in the x-y plane serves as a conduction inhibitor in the z-direction. Hence, to model the defect, the z-direction thermal conductivity was reduced between two plies over a portion of the modeled section. This introduced the concept of the "Defect Conduction Factor" (DCF), such that

$$kz_{DEFECT} = DCF \cdot k_z \quad , \tag{7}$$

where kz_{DEFECT} represents the z-conductivity at the defect and kz is from Equation (6). The DCF usually varies from 0 to 1.00. For no defect, the DCF = 1.00, while a complete delamination with no physical contact between the plies displays a DCF close to 0. Implanted defects such as the TFE ones used in the experimental effort of this program have DCF's closer to 0.5, depending on the implant material and thickness.

It is possible to characterize the thermal behavior of defects using only the DCF. Note that since the defects lie between two plies in this model, the x- and y-conductivities will be unaffected. For cases of damaged plies, rather than delaminations, the model must be revised.

NODAL EQUATIONS

Using the thermal properties derived and the concept of the defect conduction factor, it is possible to write the nodal equations

for the finite difference. As an example, the nodal equation for all internal nodes will be given here. Consider node (i,j,k), and let

$T_{i,j,k}'$ = nodal temperature at time t+Δt

$T_{i,j,k}$ = nodal temperature at time t

Δt = time interval.

Then the resulting nodal equation is

$$T_{i,j,k}' = \frac{k_{x_k}}{A}(T_{i-1,j,k}+T_{i+1,j,k}) + \frac{k_{y_k}}{A}(T_{i,j-1,k}+T_{i,j+1,k})$$

$$+ \frac{k_{z_{i,j,k-1}}\, n^2}{A}(T_{i,j,k-1}) + \frac{k_{z_{i,j,k}}\, n^2}{A}(T_{i,j,k+1})$$

$$- \frac{T_{i,j,k}}{A}\left[2(k_{x_h}+k_{y_k}) + n^2(k_{z_{i,j,k-1}}+k_{z_{i,j,k}})\right] - A$$

where $A = \rho C n^2 dz^2/\Delta t$

n = nodal aspect ratio = dx/dz

dz = nodal thickness = ply thickness.

Note that the x- and y-thermal conductivities, which were given by Equation (6) are subscribted $(\ )_k$ indicating that they have a different value for each ply. The z-conductivity must be handled in a different manner since it may change within a given ply due to the presence of a defect. Hence,

$k_{z_{i,j,k-1}}$ = conductivity at node (i,j) in ply (k) governing heat flow from ply (k-1) to ply (k).

$k_{z_{i,j,k}}$ = conductivity at node (i,j) in ply (k) governing heat flow from ply (k) to ply (k+1).

At all (i,j,k) not adjacent to the defect,

$$k_{z_{i,j,k}} = k_t \quad .$$

For defects, $k_{z_{i,j,k}} = DCF \cdot k_t$.

Associated with each nodal equation in the finite difference model is a stability criterion. For the case of Equation (8), the final bracketed term must not be less than zero or the 3rd Law of Thermodynamics will be violated. This criterion leads to the selection of a time interval for the solution

$$2(k_{x_k} + k_{y_k}) + n^2(k_{z_{i,j,k-1}} + k_{z_{i,j,k}}) - \frac{\rho C n^2 dz^2}{\Delta t} \geq 0$$

$$\therefore \quad \Delta t = \rho C n^2 dz^2 / \{2(k_{x_k} + k_{y_k}) + n^2(k_{z_{i,j,k-1}} + k_{z_{i,j,k}})\} \quad . \qquad (9)$$

In a similar manner, nodal equations such as (8) and stability criteria such as (9) can be derived for each of the different kinds of nodes. In all, there are six types of nodes used in this model:

1. Interior nodes
2. Top surface insulated nodes
3. Insulated edge (side and top) nodes
4. Insulated corner (side) nodes
5. Insulated upper and lower corner nodes
6. Bottom surface nodes with heat input

The final theoretical consideration to be discussed is the inclusion of the external thermal load in the model. Two options were desired; (1) contact heating, and (2) radiant heating. Case 1 was easily handled by imposing a boundary condition that the back surface remain at the elevated temperature of the contacting heat source. The second case necessitated the addition of an input term to the back surface nodal equation. The heat input is actually treated as an internal heat generation at the back surface only. This provides a reasonable simulation of the radiant heating without complicating the nodal equations unduely.

Program Description

A computer program was written to handle the solution of the nodal equations for the flawed composite plate. The program, called "CMHT" (for Composite Material Heat Transfer program), was written in FORTRAN IV for a Burroughs 7700 computer. The data input is interactive and free-format. A flow chart of CMHT is shown in Figure 13. More details on running the program may be found in the "User's Guide to CMHT."

FIGURE 13. FLOWCHART OF CMHT PROGRAM.

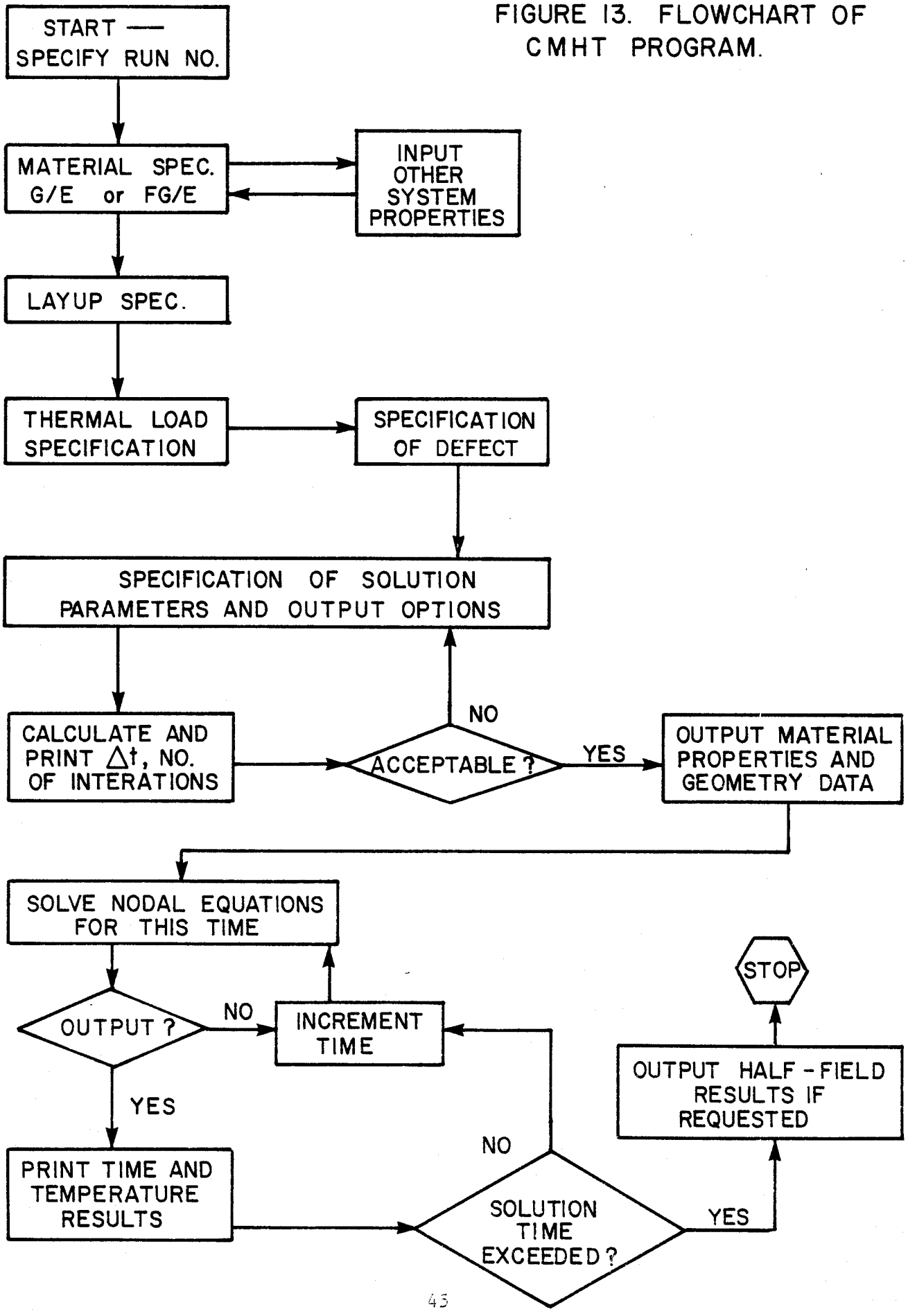

Through the interactive input, the user, responding to prompts, specifies the material system properties. Two systems are included in the program. These are graphite/epoxy and fiberglass/epoxy, whose thermal properties were taken from Ref. (8). The layup of the laminate is then specified. Options for quasi-isotropic and unidirectional are included. Figure 14 illustrates the modelling of the laminate.

The thermal conditions are then specified. These include initial uniform temperature, mode of thermal loading (contact or radiant) and the value of the load. For the case of radiant heating, the user must also specify the duration of the input. This option may be used to simulate "pulse" heating.

Next, the defect is specified. First the ply number below the defect is input. The user then specifies the size of the defect using either an internally-generated square defect or by inputting each (i,j) value in the defect separately. This allows the simulation of odd-shaped defects. Finally, the Defect Conduction Factor is input to describe the thermal behavior of the defect.

The "solution parameters' are specified next. These include the nodal aspect ratio, the real-time limit for the solution, and the number of iterations per output group. Three output options are also available. These are: (1) back center temperatures, (2) through-thickness temperatures, and (3) half-field surface temperatures.

5 - PLY LAMINATE : NPLY = 5

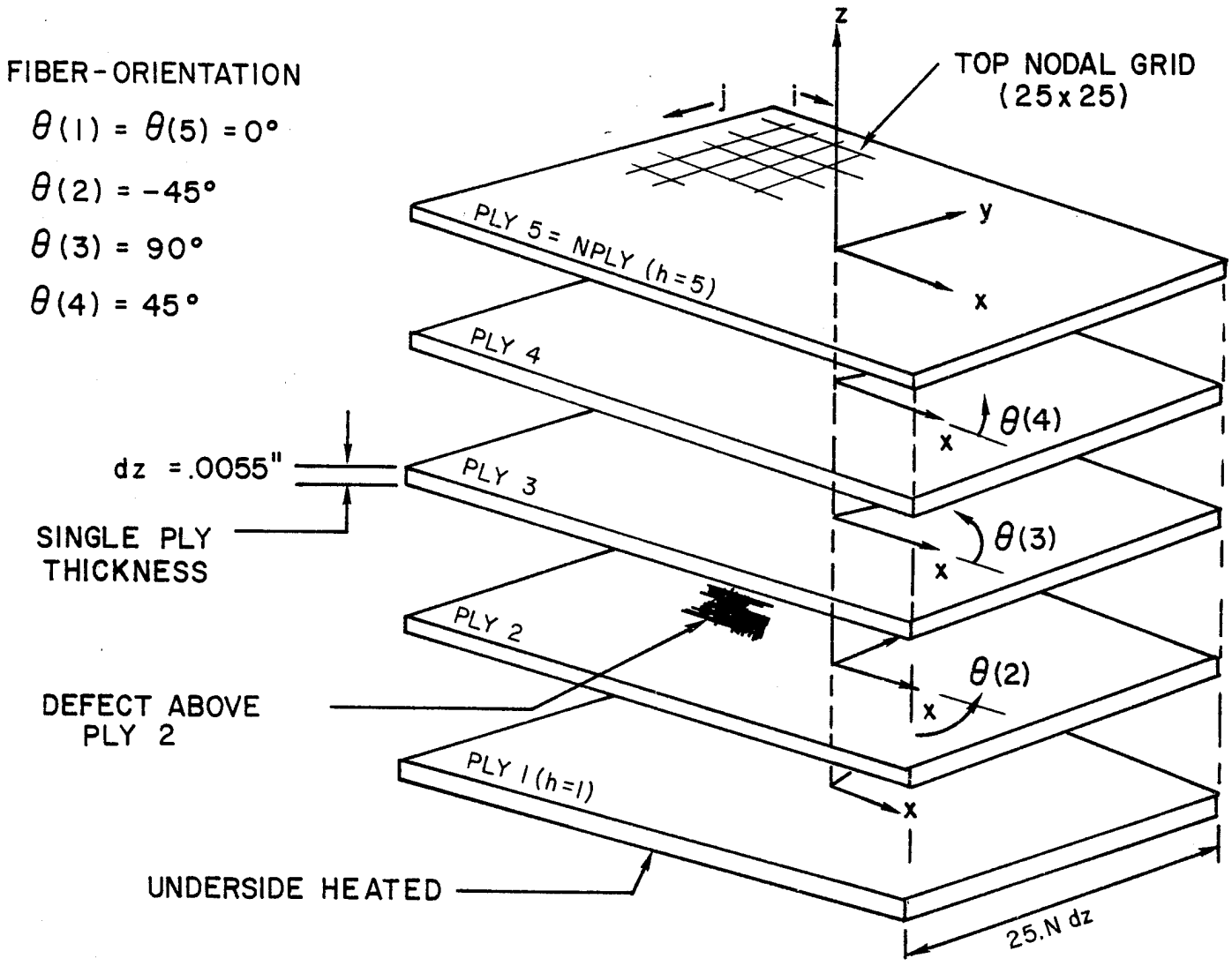

FIGURE 14. GEOMETRY USED IN PROGRAM CMHT.

This completes the data input, and CMHT proceeds to calculate the required time interval and print out the interval and number of iterations required for the solution. The user may then elect to return to reinput the time limit if desired, or specify a different number of iterations/output.

The program then solves the nodal equations at each time interval, printing output at the requested times. This output consists of the iteration number, time, "edge gradient," and x-scan of temperatures up to the specimen center. The edge gradient is the temperature gradient across the edge of the standard square defect. If through-thickness temperatures were requested, the arc inserted in the output table at the proper times. If half-field temperatures were requested, they are printed after the solution is complete.

As CMHT was run for this study, there are 25x25x8 = 5000 nodal equations to be solved for each time interval for an 8-ply specimen. For graphite/epoxy, the typical time interval was 0.008 seconds. For each real-time second, 125 iterations were required. For a 5 second run, over 3×10^6 nodal calculations are required. This large number of calculations restricted the program runs to 8-ply thicknesses (at most) and 7 seconds real-time. In all, about 90 runs were made in the parametric study. Example runs can be found in the User's Guide.

Model Verification

In order to verify the accuracy of the finite difference model, measurements of the temperature rises on graphite/epoxy and fiberglass/epoxy specimens were made and compared to predictions from CMHT. Using the bondable temperature gages described previously, measurements of both back and front surface temperatures on radiatively heated specimens were made. The results of these measurements are shown in Figure 15.

CMHT was run for 8-ply, quasi-isotropic G/E and FG/E models with no defects (i.e., using a DCF = 1.0). By a trial and error process, the intensity of the heat input and the thermal conductivities of the matrix materials were found which yielded excellent agreement between the model and the experimental results. The comparisons are shown in Figures 16 and 17. The results lend credence to the model, and give one confidence in its use for a parametric study. It should be noted, however, that for other heat sources or materials some similar comparisons and property adjustments must be made to ensure the model's accuracy.

Parametric Study Results

Using the verified numerical model, a parametric study was performed to investigate the effects of various parameters on the expected resolution of the image. Therefore, the temperature gradient across the edge of the defect (called the "edge gradient") was of

FIGURE 15. MEASURED TEMPERATURE RISES FOR RADIENT HEATING.

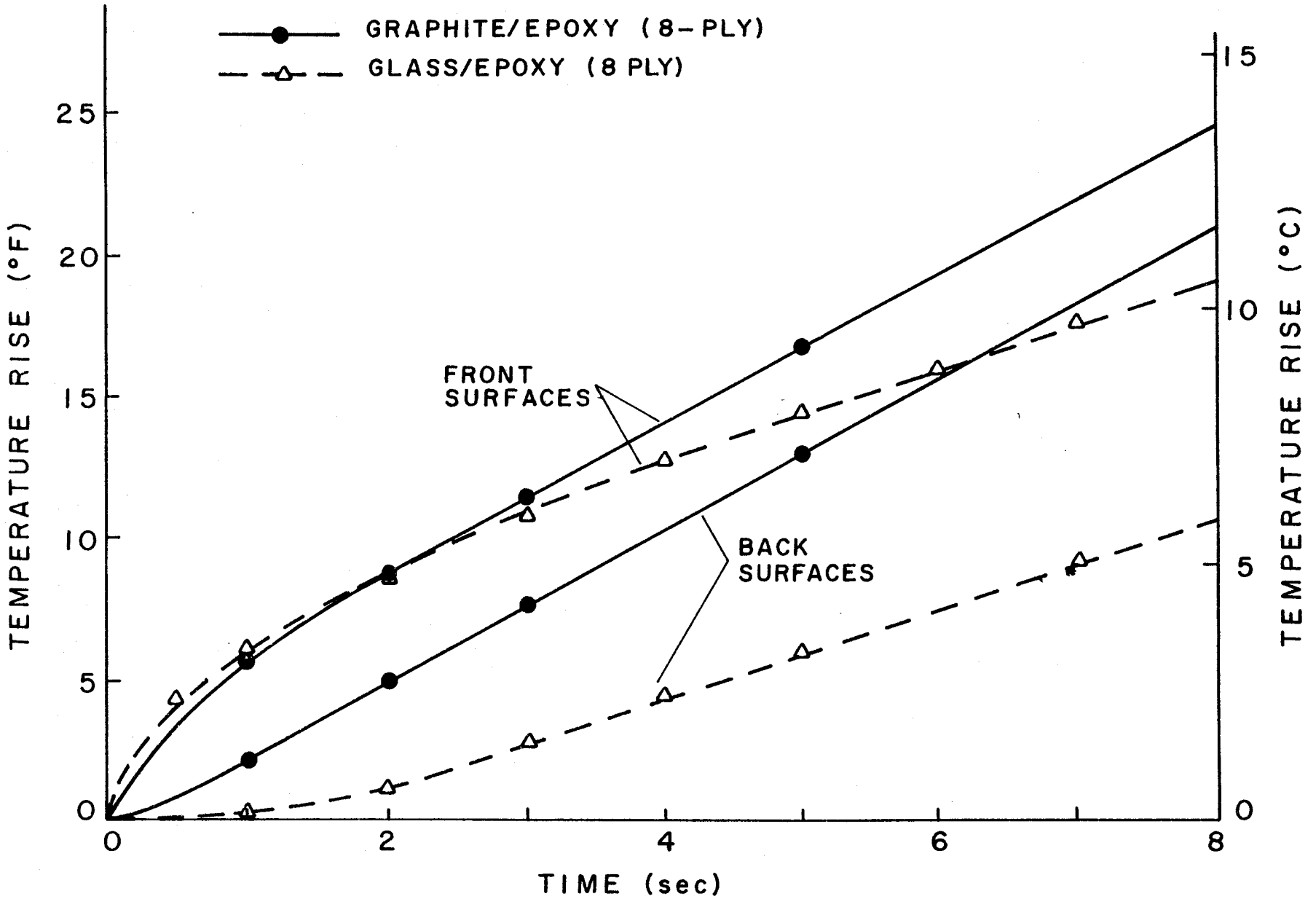

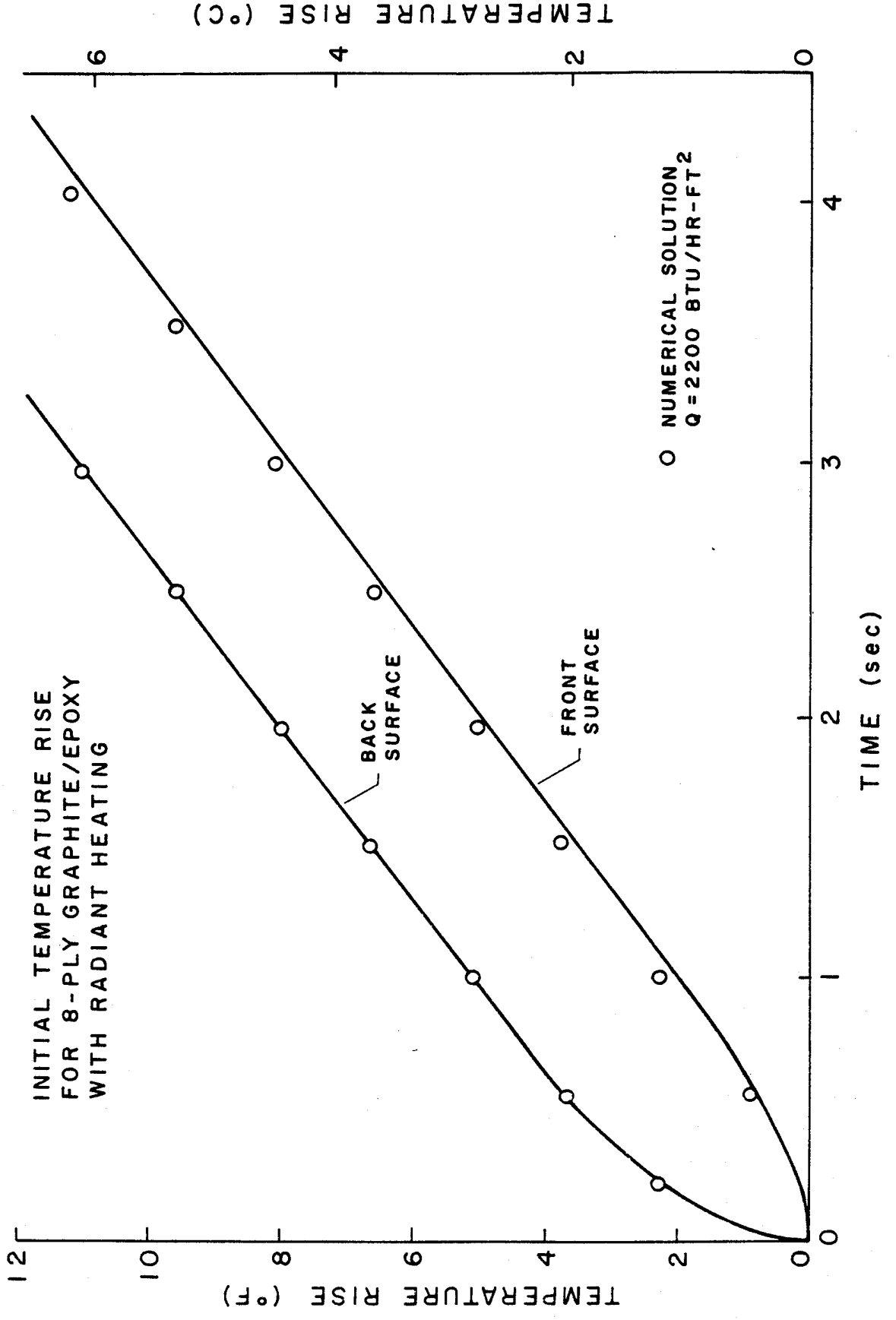

FIGURE 16. COMPARISON OF EXPERIMENTAL AND NUMERICAL RESULTS FOR GRAPHITE/EPOXY.

FIGURE 17. COMPARISON OF EXPERIMENTAL AND NUMERICAL RESULTS FOR FIBERGLASS/EPOXY.

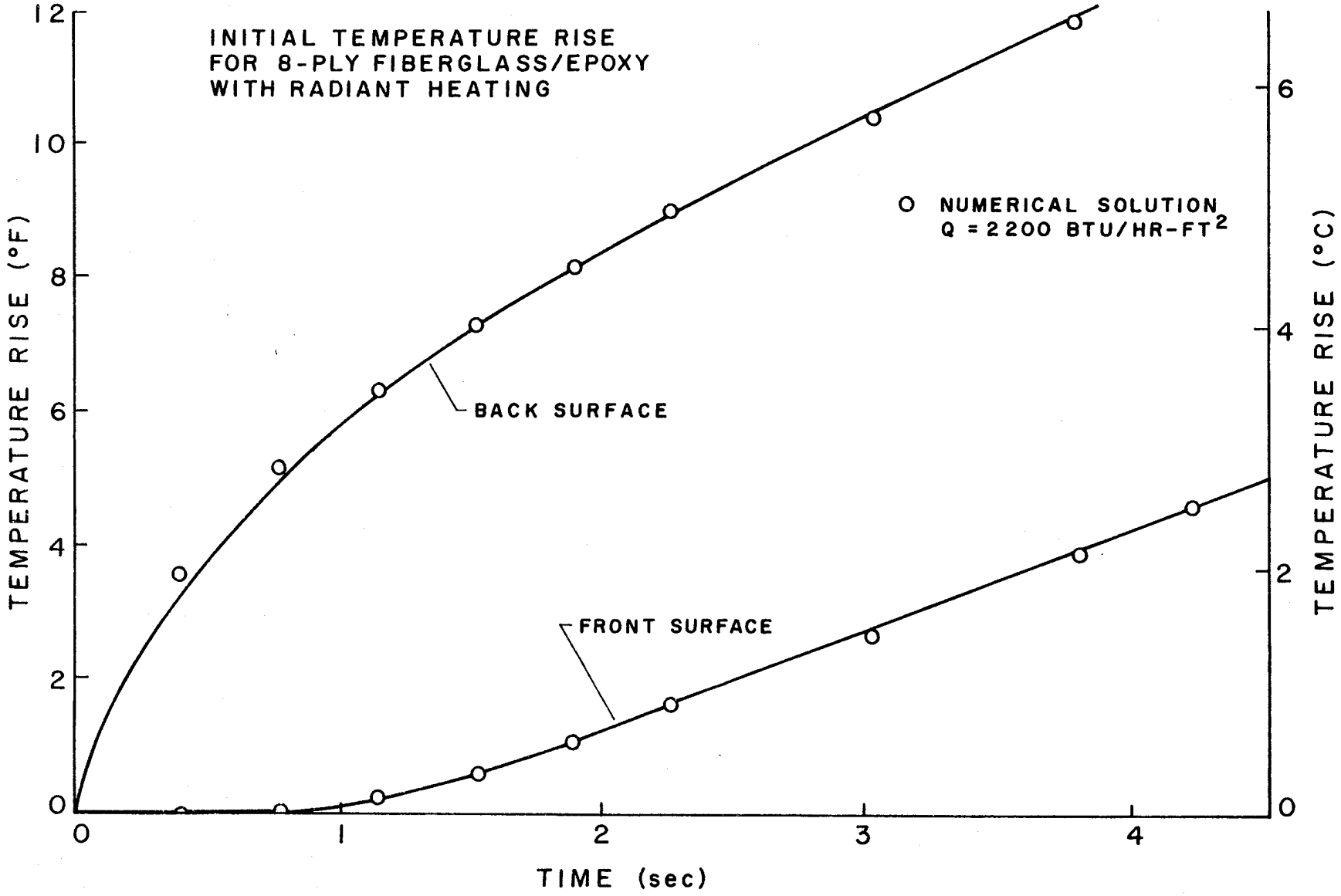

primary concern. Given that liquid crystals are obtainable for any desired temperature level, the magnitude of the temperature rise itself only serves to help identify which imaging compound should be used. While this is important, it is the magnitude of the edge gradient which serves to produce the color variations around the defect and render it visible. Higher gradients will lead to greater resolution of the defect, while low gradients may cause the image to become "smeared" out. Hence, the edge gradient becomes the primary dependent variable in this study.

Before examining the gradient results, it may be interesting to note just how the temperature distribution in the specimen develops. Figures 18-20 show the development of the through-thickness temperature profiles in G/E, flawed material. The profiles are taken through the center of a 0.35" (8.89 mm) defect. Figure 18 shows the case of a "perfect" flaw (Defect Conduction Factor = 0) in an 8-ply G/E laminate heated by contact with a 100^{o}F (37.8^{o}C) surface. Figure 19 shows the same geometry and heating but assumes a DCF = 0.5, which is more reasonable for implanted TFE defects. Note that the effect of the defect is considerably less in Figure 19. Finally, Figure 20 shows the same system (with DCF = 0.5) under a radiant thermal load. It can be seen that the back temperature can rapidly become quite high under radiant heating.

Figure 21 illustrates the development of surface temperatures in G/E under contact heating conditions. Plotted are surface temperature rises above the initial condition along the x-axis across the defect

FIGURE 18. DEVELOPMENT OF THROUGH-THICKNESS TEMPERATURE PROFILES FOR "PERFECT" FLAW WITH CONTACT HEAT.

T(BACK) = 100

PROFILES TAKEN
AT DEFECT CENTER

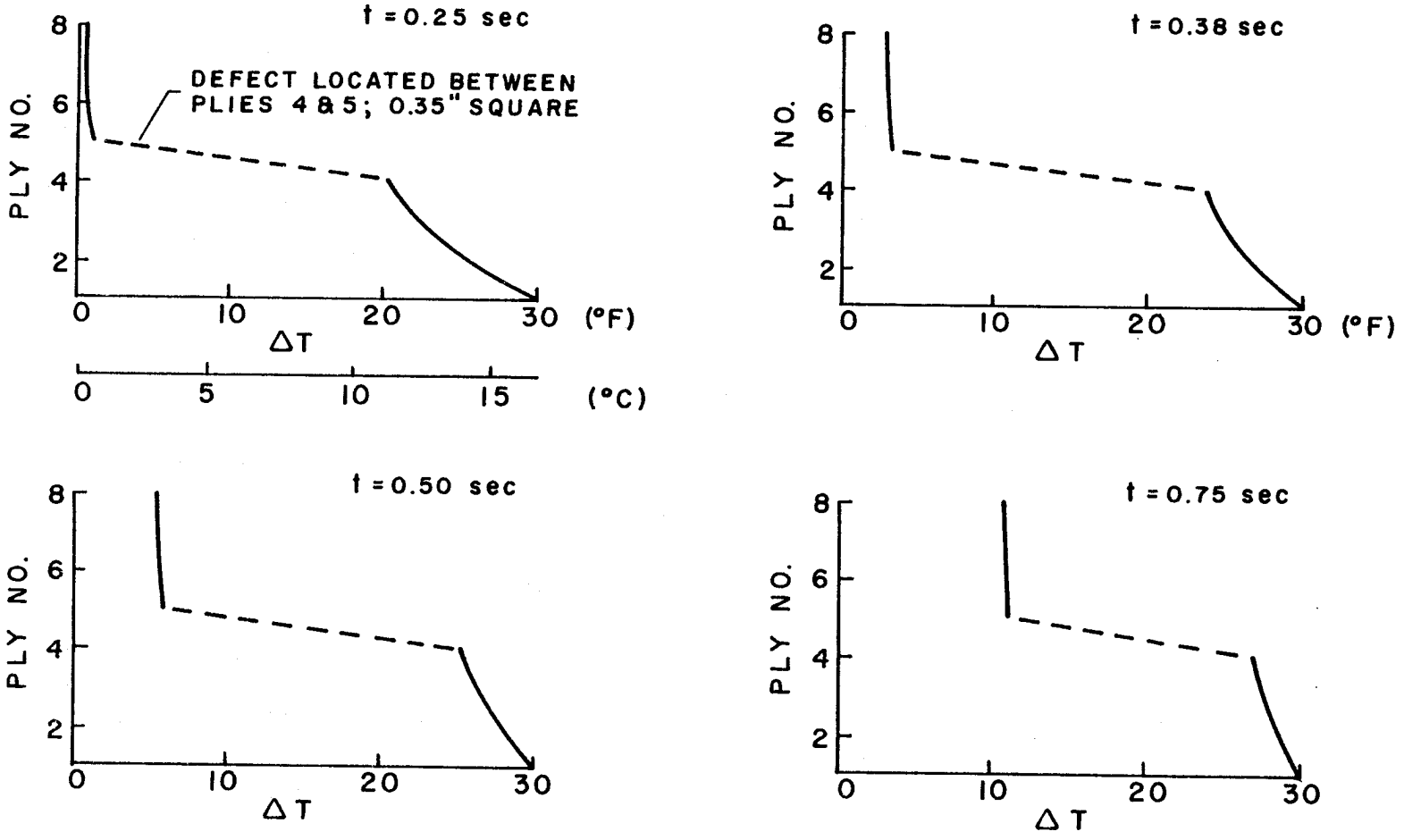

FIGURE 19. DEVELOPMENT OF THROUGH-THICKNESS TEMPERATURE PROFILES FOR CONTACT HEATING OF G/E LAMINATE.

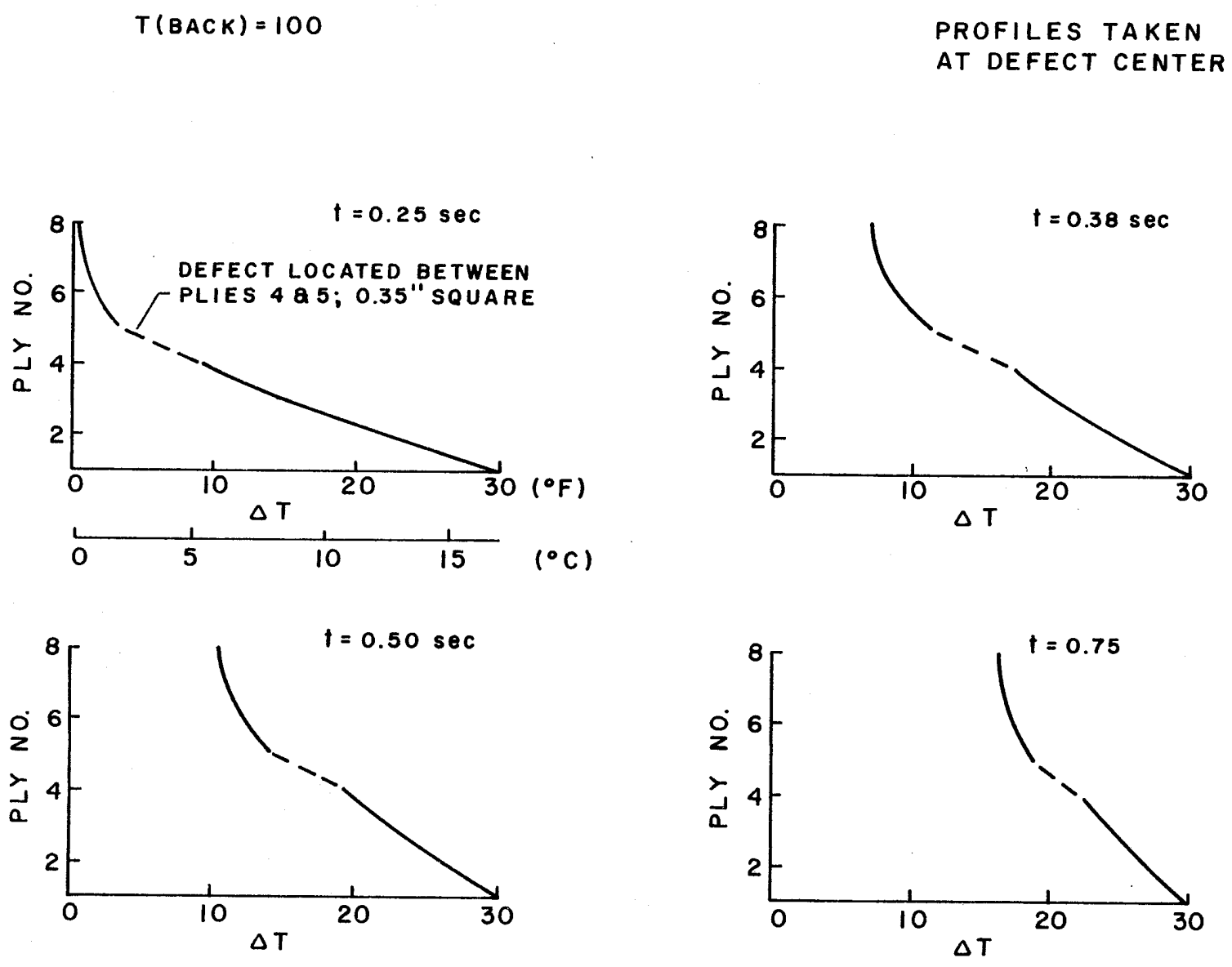

FIGURE 20. DEVELOPMENT OF THROUGH-THICKNESS TEMPERATURE PROFILES FOR RADIANT HEATING OF G/E LAMINATE.

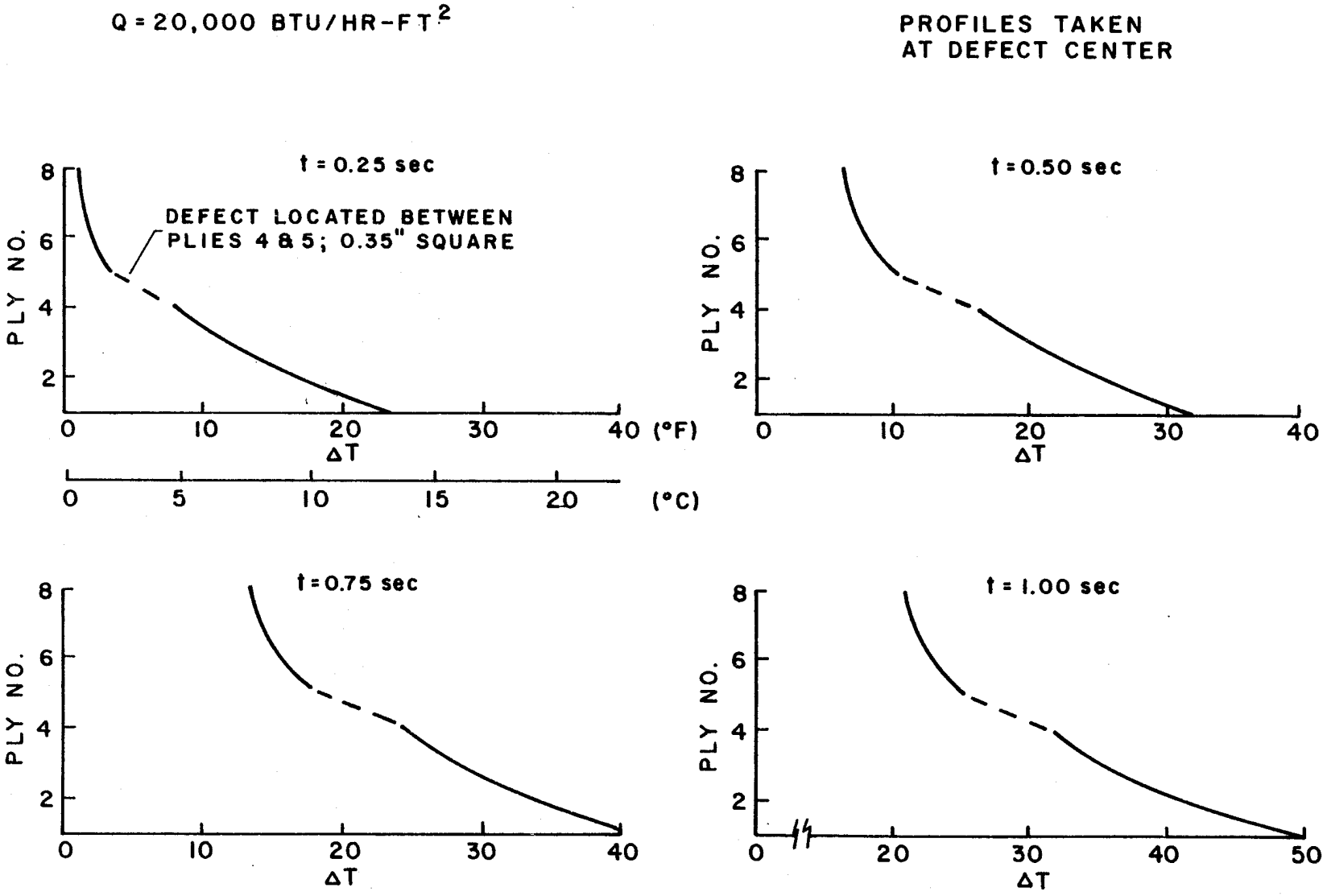

FIGURE 21. DEVELOPMENT OF SURFACE TEMPERATURES AND GRADIENTS FOR GRAPHITE/EPOXY, CONTACT HEAT

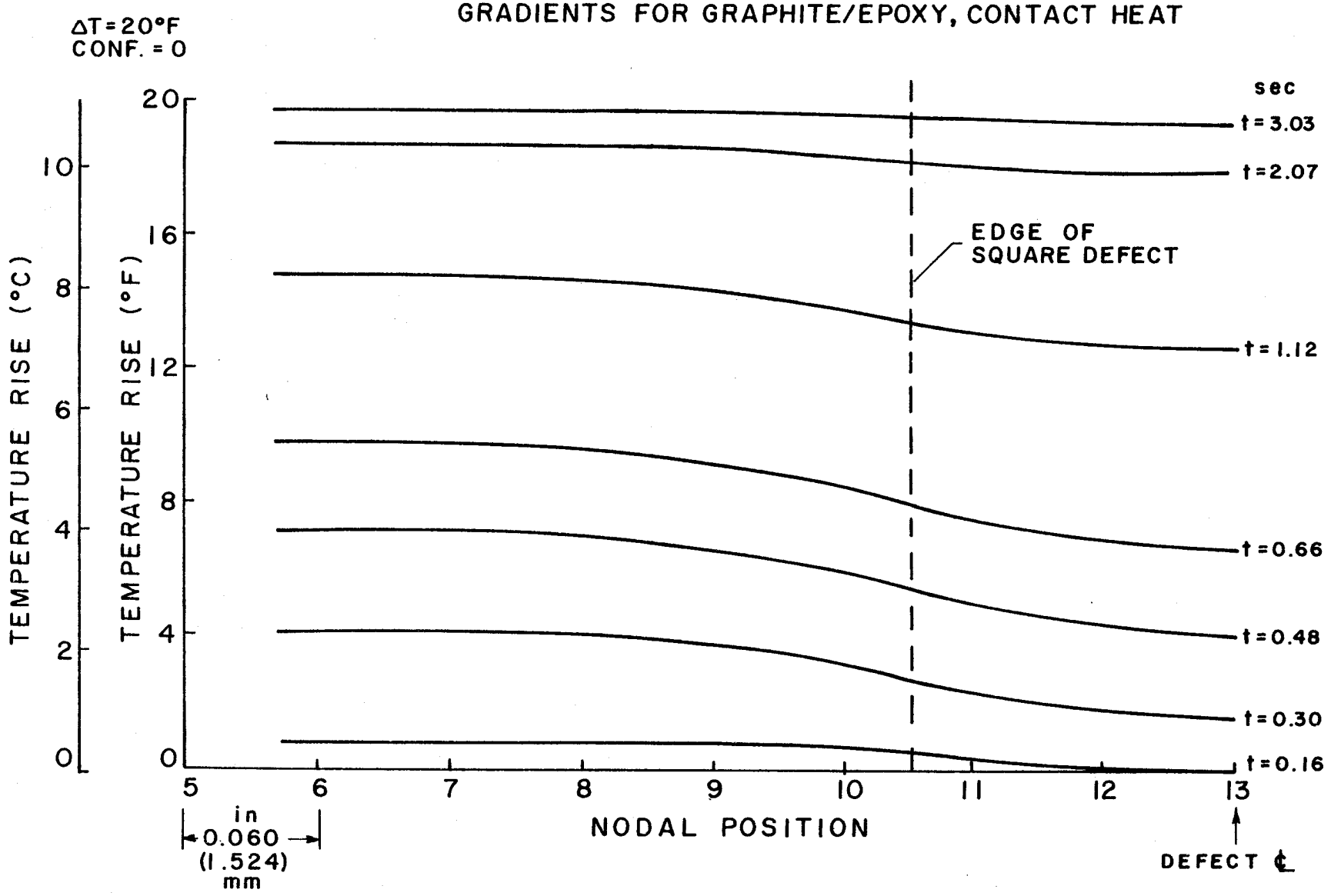

edge. One can see that in a brief period (< 3 sec) the defect, located in the middle of the 8-ply laminate, is imaged by a surface temperature gradient which reaches a maximum at about 0.5 sec, when the temperature rise is 6 - 10°F (3.3-5.6°C). By using an LC which was active at this absolute level, one could produce the sharpest image of the defect. On the other hand, using a system which imaged over 20°F (11.1°C) above room temperature would yield no indication of a defect whatsoever. This points up the potential function and value of the CMHT model. By characterizing the heat source, defect conduction factor, and thermal properties of a material to be tested, one can select the LC (or other imaging system) necessary to obtain optimum results.

Many vairables affect the surface temperature gradients to be expected using passive thermal testing of composites. Some of these are illustrated in the following figures.

The effect of the mode of thermal loading used on the edge gradients is shown in Figure 22. The relative magnitude of the temperature rises are not important, since changing the intensities of the inputs will alter that behavior. However, the shapes of the curves are important. In particular, it can be seen that radiant heating produces a more gradual change in the gradient compared to contact heating. This allows a longer time at "high gradient" on the surface, perhaps yielding a better image as the LC undergoes greater color change. It can also be seen that contact heating is generally faster than radiant heating. However, one must assure a uniform contact with the heat source to duplicate these results experimentally. Because of the difficulty of this, most

FIGURE 22. EFFECT OF MODE OF THERMAL LOADING ON GRADIENT IN GRAPHITE/EPOXY.

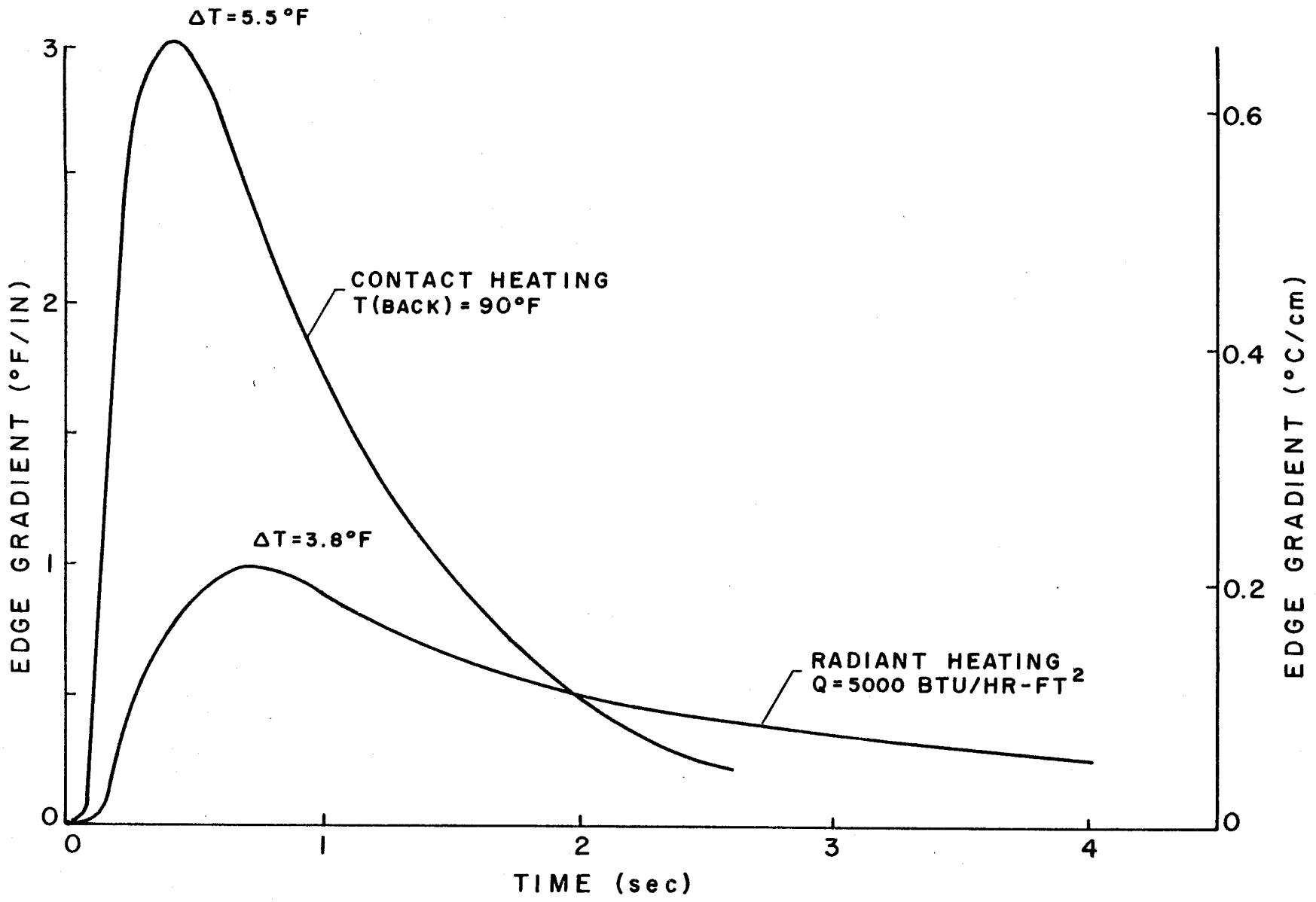

of the parametric study involved radiant heating. This also allowed a better comparison with the experimental results discussed previously.

Figure 23 shows the important effect of the intensity of the radiant input on gradients in G/E. Significant improvements in edge gradient can be achieved by using strong heat inputs compared to weak ones. This result was used in the experimental study when an early, weak heat source failed to image any but the largest defects. Changing to a stronger source yielded the clear images already discussed.

The importance of the material system tested is illustrated in Figure 24. For the same heat input, 8-ply specimens of G/E and FG/E with 0.30" (7.62 mm) defects exhibit significantly different gradients. This is due to the differences in the thermal properties of the two systems. Based on these results, one could expect significantly better image definition using low-conductivity systems, compared to G/E.

One of the most important parameters in thermal NDT is the defect conduction factor. Unfortunately, it is also the most difficult to quantize (except for full delaminations where CDF=0). The effect of the DCF in G/E is shown in Figure 25. The reduction in peak edge gradient as DCF increases is significant, since it implies that some defects may go undetected if the DCF is too high. The sensitivity of the imaging system becomes more critical as the defect conduction factor increases. The DCF also effects the temperature rise at peak gradient, since more perfect defects take longer to produce peak gradients, as can be seen from the figure.

FIGURE 23. EFFECT OF RADIANT INPUT ON GRADIENT IN GRAPHITE/EPOXY.

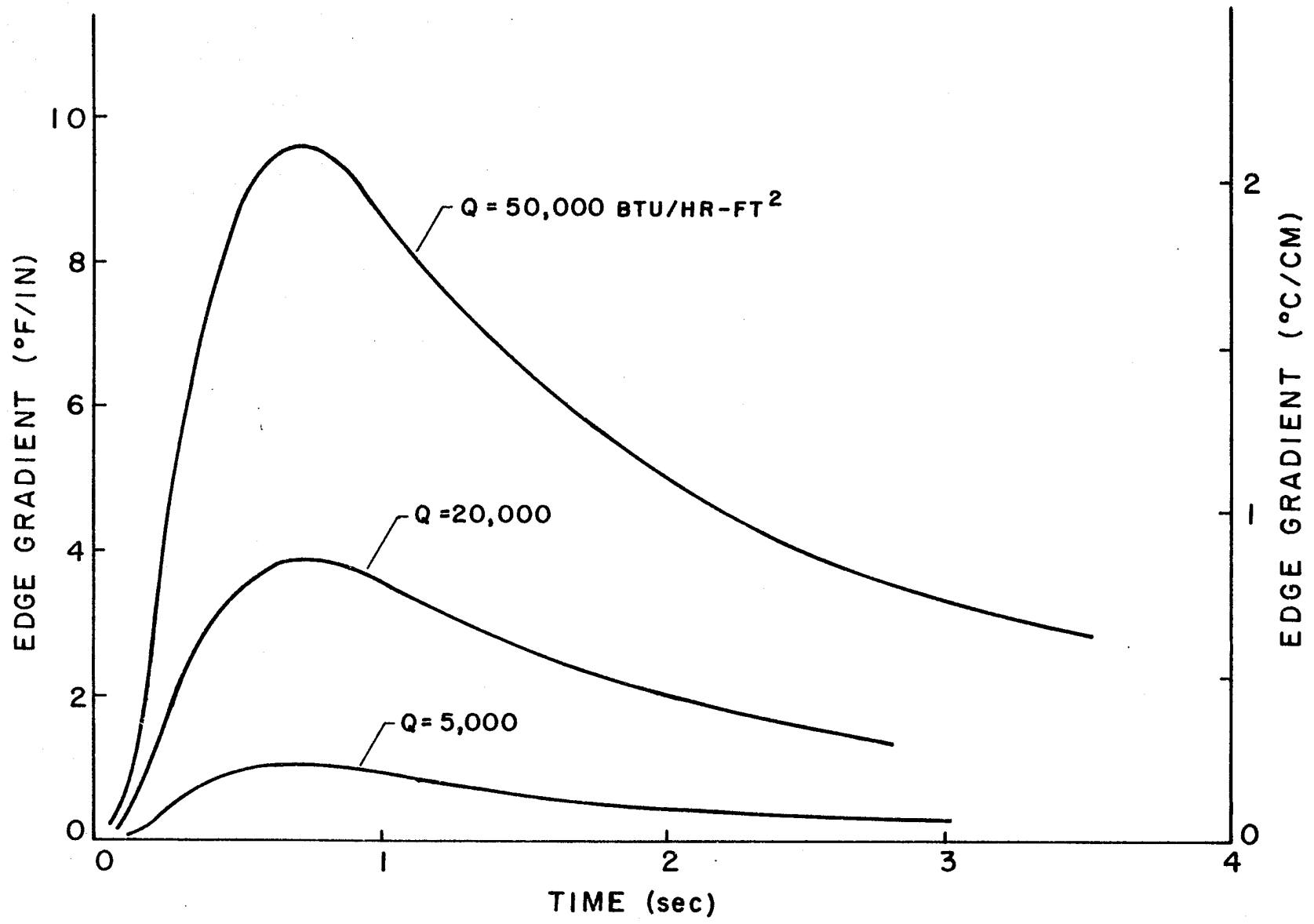

FIGURE 24. EFFECT OF MATERIAL SYSTEM ON GRADIENT AND RESPONSE TIME.

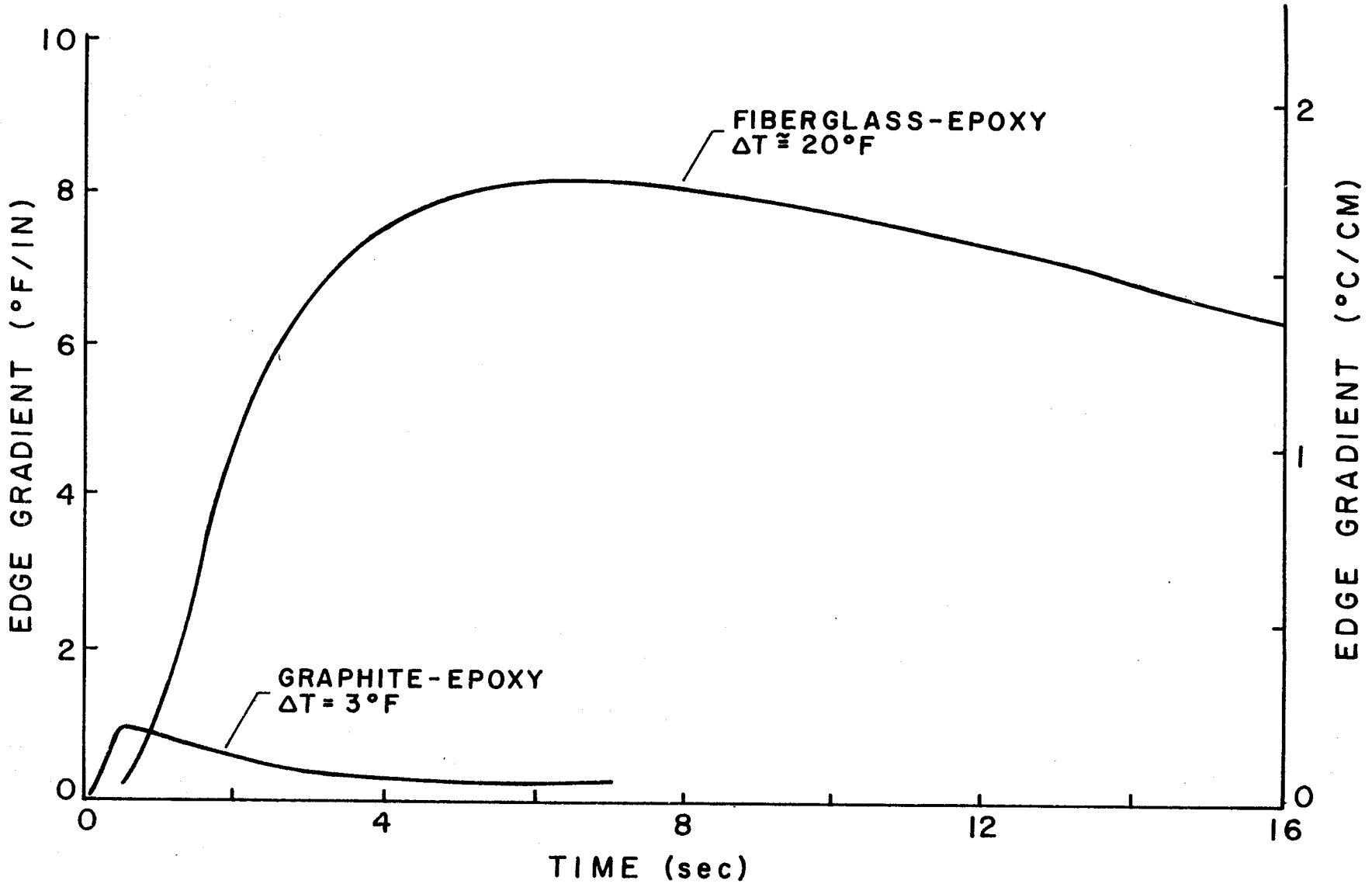

FIGURE 25. EFFECT OF DEFECT CONDUCTION FACTOR ON GRADIENT AND TEMPERATURE RISE IN GRAPHITE/EPOXY.

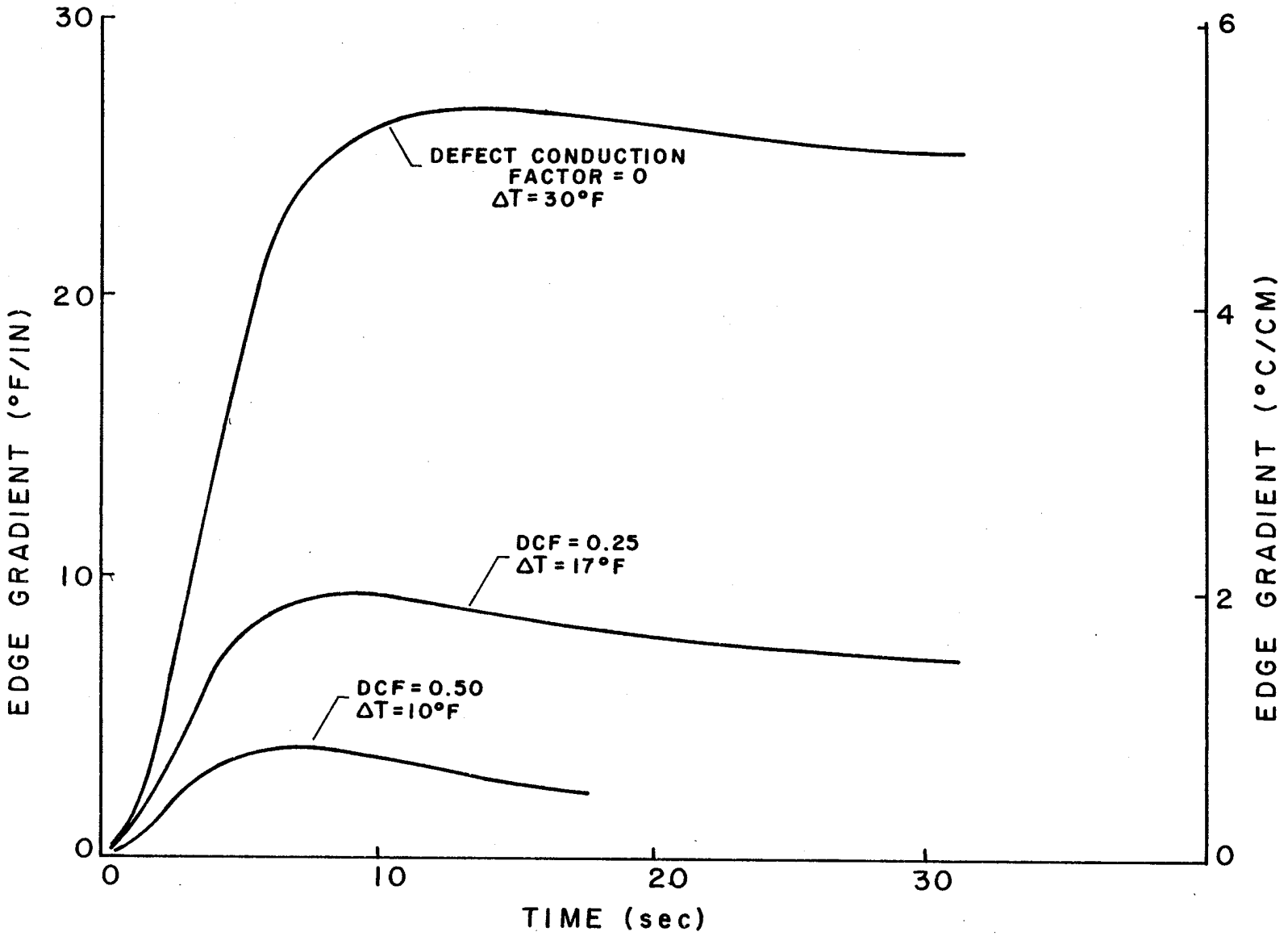

The effect of flaw depth in unidirectional G/E is illustrated in Figure 26. Note that defects just below the surface are not imaged as well as those slightly deeper. One might speculate that this may be true only for the case of DCF = 0.5 shown here. A perfect defect (DCF=0) might produce the best image when it is just below the surface, and the image should get progressively worse as the depth increases. However, similar behavior was noted in cases run with DCF=0. It should also be noted that the peak gradients occur at essentially the same temperature rise regardless of flaw depth.

The effect of flaw size is shown in Figure 27. As would be expected, smaller defects produce lower surface gradients than large defects do for constant heat inputs. As has been pointed out, increasing the heat input intensity leads to higher gradients and better flaw definition in any case.

Figure 28 illustrates the effect of laminate thickness (number of plies) on the peak edge gradient of a defect in both G/E and FG/E material systems. The defects were all taken to lie at the mid-plane of the laminates.

In the case of the G/E, multiple defect specimen shown previously in Figure 8, it was noted that the defect images tended to "neck down" in the fiber direction. This is due to the relatively high longitudinal conductivity of G/E and can be illustrated with the numerical model. Figure 29 shows gradients for 90° and 0° unidirectional laminates, and a $\pm 45^{\circ}$ orthotropic laminate. Recalling that the

FIGURE 26. EFFECT OF FLAW DEPTH IN G/E.

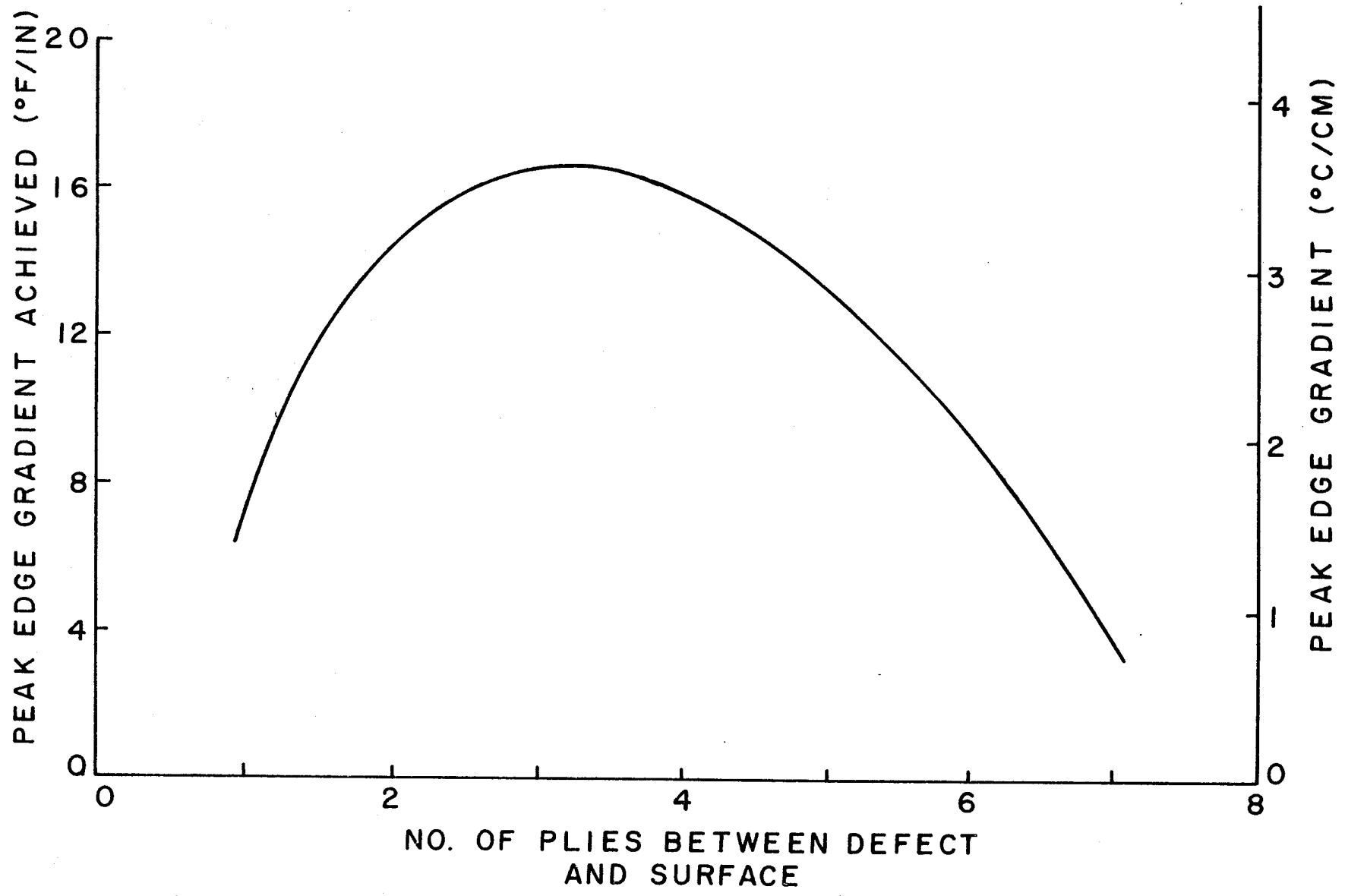

FIGURE 27. EFFECT OF FLAW SIZE ON GRADIENT IN QUASI-ISOTROPIS GRAPHITE/EPOXY.

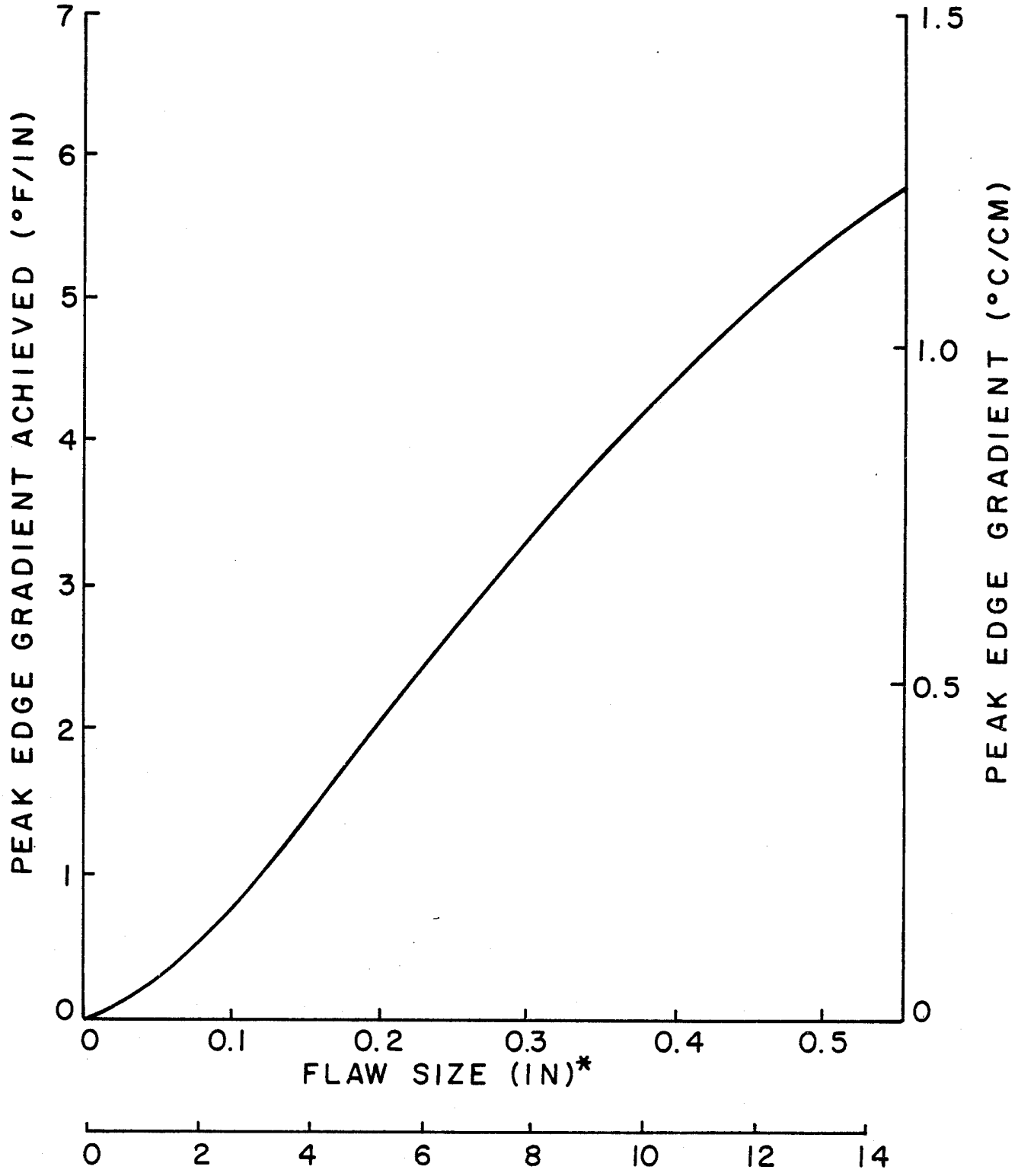

FIGURE 28. EFFECT OF NUMBER OF PLIES.

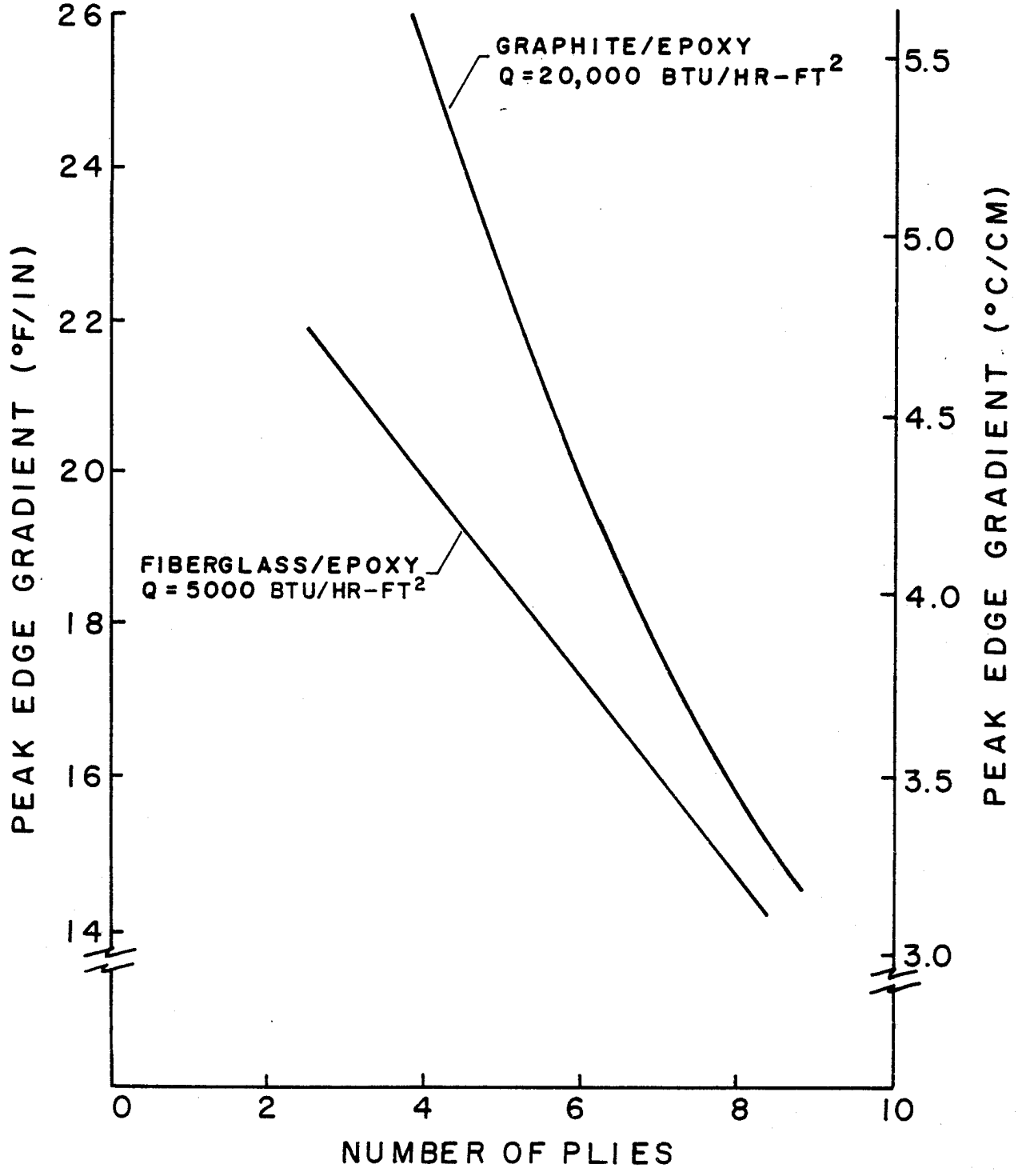

FIGURE 29. EFFECT OF LAYUP ON GRADIENT IN GRAPHITE/EPOXY LAMINATE.

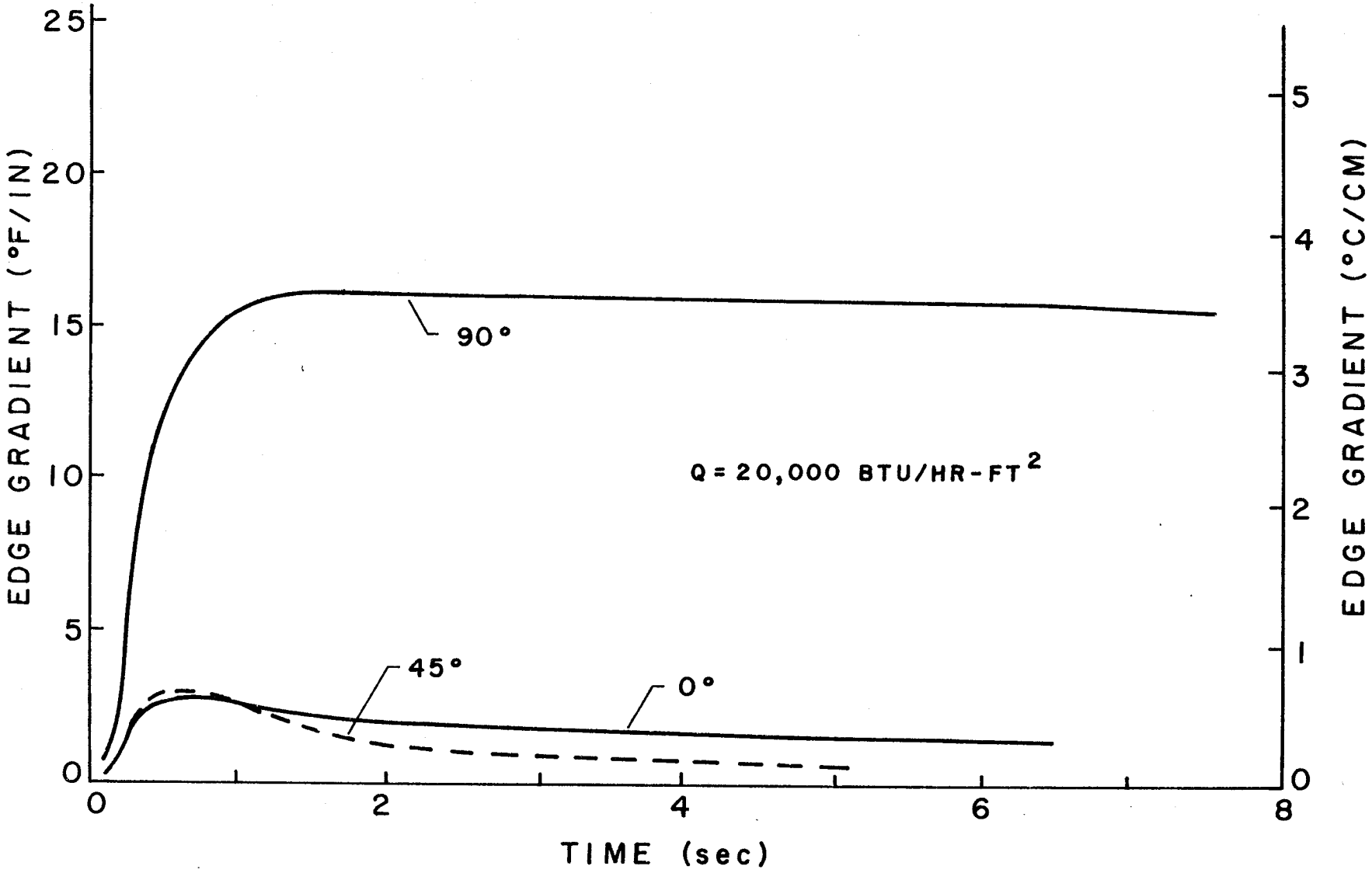

gradients calculated by the model are only x-direction gradients, the two unidirectional cases can be construed to be transverse and longitudinal gradients of a single unidirectional laminate. The relative magnitude of the two curves, and the more rapid decrease of the 0^{o} (longitudinal) curve, explains why the defect images appear to neck down in the longitudinal direction and retain shape transversely.

The remaining figures to be discussed illustrate similar aspects of the effect of heat input, conduction factor, and defect size for the case of contact heating. Figure 30 shows how the gradients may be improved by increasing the heat input. Figure 31 shows once again the pronounced effect of the defect conduction factor on the gradients. Figure 32 illustrates the effect of defect size on the peak edge gradient for the case of contact heating. Note that in the case of defect size, the time to peak indication is also influenced.

FIGURE 30. SURFACE TEMP. GRADIENTS EFFECT OF BACK TEMP.

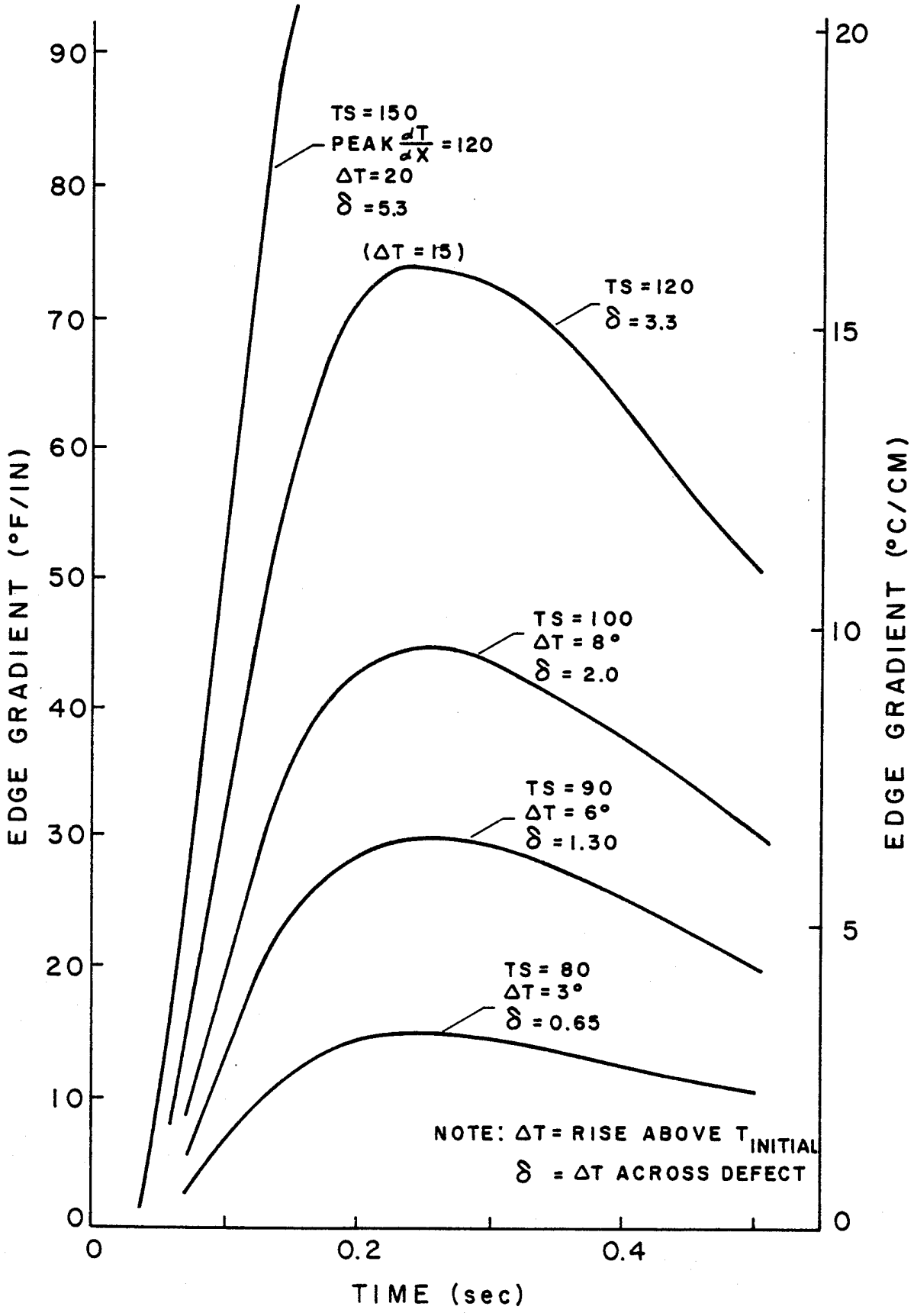

FIGURE 31. EFFECT OF DEFECT CONDUCTION FACTOR ON MAX. GRADIENT.

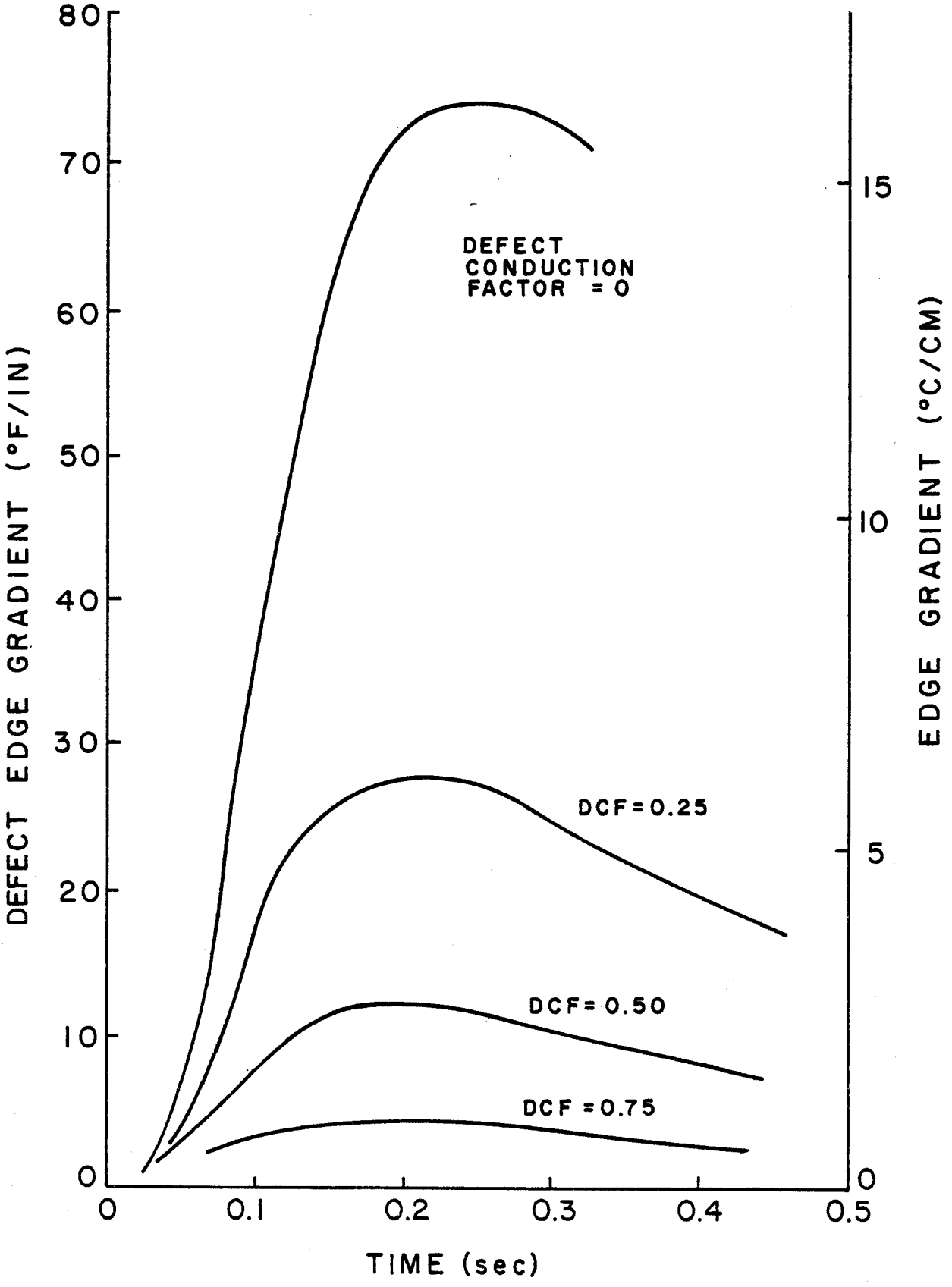

FIGURE 32. EFFECT OF DEFECT SIZE ON MAX. SURFACE GRADIENTS.

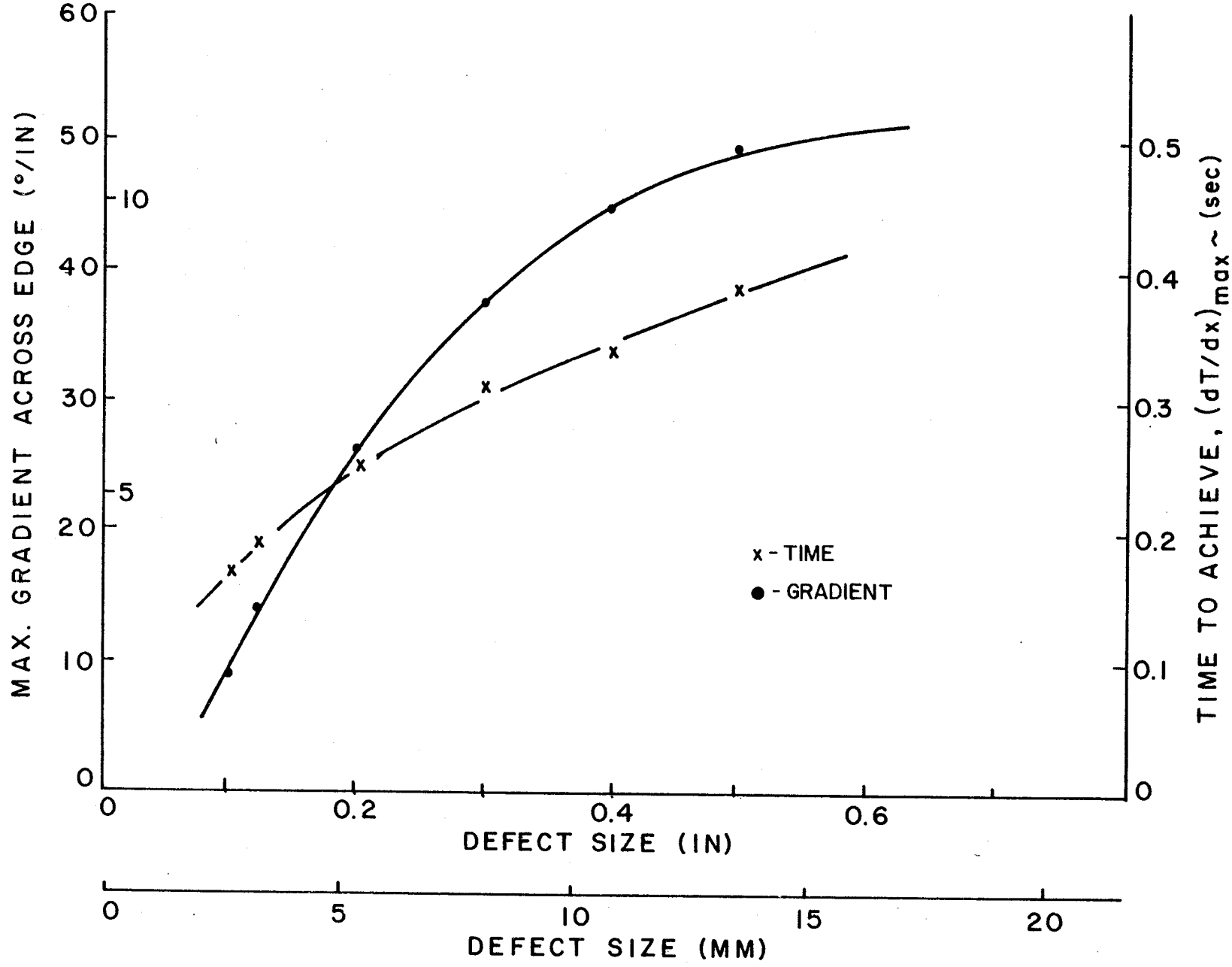

CONCLUSIONS AND RECOMMENDATIONS

In this study, the potential use of liquid crystal thermography for nondestructive inspection of composite materials has been investigated. It has been shown through the experimental program that defects of various sizes and geometries can readily be imaged using the techniques developed here. Furthermore, through the use of numerical modeling techniques, a parametric study has been performed to identify the critical variables in the process and assess their impact on the results.

Specifically, this study has accomplished the following objectives:

- Develop a reliable technique for applying a high-quality coating of liquid crystals to the test material.
- Develop an understanding of heating techniques and their effect on the image produced.
- Refine data-taking procedures, including the addition of time data.
- Demonstrate the use of thermal imaging to locate implanted defects in G/E and FG/E.
- Quantify the effect of LC imaging system on response time for laminates of different thicknesses.

- Develop and verify an analytical model of the passive thermal NDT process.
- Utilize the model to identify important variables in the process, such as heat input, flaw size, material matrix conductivity and laminate layup.
- Demonstrate the application of passive LC thermography for the inspection of bonded joints.
- Demonstrate the ability of passive LC thermography to detect manufacturing flaws in short-fiber composite sandwich structures.

While these results have been very promising, the widespread use of passive thermal imaging of composites in industrial situations will require an even better understanding of the process. Several areas for further investigation were suggested through the experiences in this study. These include:

- Development of better heat sources for both radiant and contact heating.
- Experiments with different LC imaging systems (of wider range or more uniform sensitivity).
- Application of other electronic imaging systems in the passive NDT process.
- Investigation of visualization of natural defects rather than implanted ones.

- Thermal characterization of different types of defects through the defect conduction factor.
- Improvements to the analytical model to better represent the passive thermal NDT process.

Passive thermal NDT of composite materials shows greater potential for industrial application due to its low cost, high speed, and relative ease of use. Through this study, passive LC NDT has come much closer to this application. With further study, passive thermal nondestructive testing of composites will undoubtedly become an important part of the growing composites industry.

REFERENCES

1. Reifsnider, K. L. and Williams, R. S. Experimental Mechanics, Vol. 14, No. 12, Dec. 1974, pp. 479-485.

2. Charles, J. A., Appl, R. J. and Fransis, J. E. Journal of Engineering Materials and Technology, Vol. 100, No. 2, March 1978, pp. 200-203.

3. Charles, J. A. "Liquid Crystals for Flaw Detection in Composites," ASTM Committee D-30 Conference on NDE and Flaw Criticality for Composite Materials, Philadelphia, PA., Oct. 10-11, 1978.

4. Henneke, E. G., II and Jones, T. S. "Detection of Damage in Composite Materials by Vibrothermography," ASTM Committee D-30 Conference on NDE and Flaw Criticality for Composite Materials, Philadelphia, PA, Oct. 10-11, 1978.

5. Brontman, J., Kobayashi, T., and Carrillo, D. Journal of Composite Materials, Vol. 3., Oct. 1969, pp. 702-704.

6. McLaughlin, Phillip V., Jr., McAssey, V., Dietrich, R. C., "Non-Destructive Examination of Fiber Composite Structures by Thermal Field Techniques," 34th Annual Technical Conference, 1979 Reinforced Plastics/Composites Institute, The Society of the Plastics Industry, Inc., Section 22-D, pp. 1-11.

7. Whitcomb, J. D., "Thermographic Measurement of Fatigue Damage," Composite Materials: Testing and Design (Fifth Conference), ASTM STP 674, S. W. Tsai, Ed., American Society for Testing and Materials, 1979, pp. 502-516.

8. Materials Selector, 1974, Vol. 80, Number 4.

APPENDIX

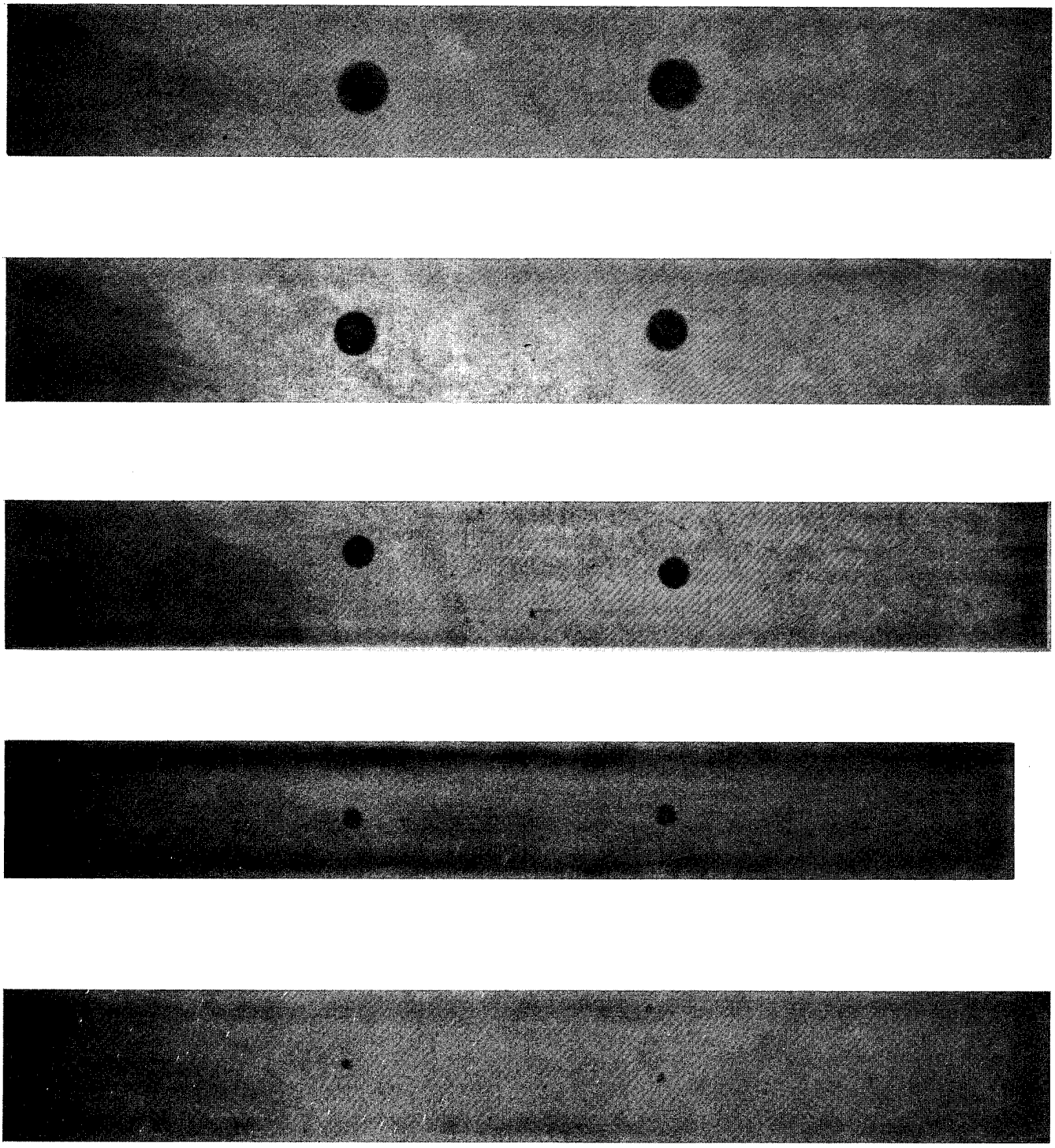

ULTRASONIC C-SCANS OF 8-PLY QUASI-ISOTROPIC GRAPHITE/EPOXY SPECIMENS CONTAINING TFE IMPLANTED DEFECTS.